Proposal for Supporting Beamline 6BMB at APS

PI. Donald J. Weidner, co-PI. Matthew Whitaker
Stony Brook University

Executive Summary

X17B2/6BMB/XPD is a research and techniques development beam line program led by Stony Brook (PI: Weidner) in collaboration with Stony Brook staff and the PIs of the Rheology Grand Challenge (Karato, Durham, Wang, and Burnley). Through its on-going efforts in techniques development, the beam line has nucleated the entirely new research field of *in-situ* studies of rock deformation. These world-leading development efforts include the creation of the D-DIA apparatus, the RDA, and the conical slit diffraction system, many of which have been adopted at beamlines around the world. Along with these instrument developments have also come a host of different strategies and techniques for using the equipment to measure a variety of physical properties and to interpret the new streams of data that these instruments produce.

These development efforts have led to many scientific accomplishments and discoveries both at the beam line and at other beamlines where our instrumentation and techniques have been adopted. Our user program, in particular, has significantly improved understanding of flow in the upper mantle by characterizing the rheology of olivine and pyroxene at appropriate pressures and temperatures, characterizing texture development, and studying the effects of changing chemistry including water and iron. The rheology of and texture development in wadsleyite and ringwoodite have also been characterized and an important strength contrast between bridgmanite and (Mg,Fe)O has been discovered. The rheology of other planetary materials such as ilmenite-olivine aggregates and Fe-rich olivine have also been investigated. These studies have implications for mantle dynamics (on Earth as well as for the Moon and Mars), the formation and isolation of geochemical reservoirs and the distribution of seismic anisotropy. Recent studies of other transport properties such as changes in the thermal diffusivity caused by the perovskite to post-perovskite phase transition also have important implications for mantle dynamics. Studies of solid-melt interactions throughout the mantle have implications ranging from the degree to which molten iron in the outer core penetrates into the mantle to the degree to which dynamic partial melting causes seismic wave attenuation. Other studies span a wide range of topics from brittle deformation of quartz to the formation of tissinite in meteorites.

This beamline program was located at the NSLS X17B2 until the NSLS shut down and is now in a state of transition; located at APS 6BMB and NSLSII XPD. For the long term we need a platform with a large, high flux white beam source and ample hutch space for existing equipment as well as apparatus that will be developed in the future. Due to the strong scientific synergy between low and high pressure deformation, we anticipate that our techniques can make significant contributions to low pressure brittle deformation and fluid interaction studies in the future and we desire the flexibility to accommodate this work. We see the new HEX beam line at the NSLS II as the place most likely to provide a good home for our future efforts. They will have world class white beamlines with dimensions as large as 25 mm high (the smallest dimension), ideal for 3-D imaging rock samples. While HEX is in development, we seek to maintain the facilities and staff support at 6BMB in order keep our user community's science flourishing.

1. Introduction

In this proposal, we are asking for support of the 6BMB beamline at the APS for another year, with the possibility of continuous funding for the next few years. This beamline has a heritage that goes back to the early 1990's when a superconducting wiggler was installed at the NSLS. CHiPR negotiated for a small amount of the beamtime to use a newly acquired DIA. From that early time onward, the beamline has evolved tremendously, capturing and inventing new techniques, as it pursued new scientific missions that were amenable to high pressure synchrotron studies. At the time that the NSLS closed down, the beamline, by most measures, was the world – leading synchrotron beamline for measuring mechanical properties of Earth materials. It used about 67% of available time, employing 2 beamline scientists, with significant support from Stony Brook University. The hutch was equipped with a DDIA or RDA on a white beam and an experimental DT10 on a monochromatic side station. After the close of NSLS, we acquired commitments from NSLS II and APS that would provide a white beam for the DDIAand RDA (at 6BMB) and a monochromatic beam for a new DT25 at XPD at the NSLS II. The total beamtime is at least the same if not more than we had at NSLS, and the total beamline scientist support from COMPRES was the same as at the NSLS. The 6BMB beamline has been operational for over 2 years and the XPD station at the NSLS II is anticipated to be completed by the end of the year.

Mechanical properties, as we use it here, represent properties that reflect the relationship between stress, strain, and time. The elastic properties that define elastic wave speed, stand at one end of the spectrum, where no permanent deformation is inflicted on the sample, while plastic flow laws represent the other end with the sample shape changing through time. The elastic properties translate to seismic velocities and are the necessary basis that turns seismic diagrams, coded in red and blue, into temperature or compositional gradients, or that allow us to map out phase transitions as a function of depth. Plastic properties are the agent of flow that enables plate tectonics on the one hand, and leads to earthquakes on the other.

The current facility (including 6BMB and XPD) represents the leading edge for mechanical studies at this time. While we were the developers of the first high pressure, synchrotron based, deformation machine (the DDIA), many other synchrotrons have adapted this system. However, we are the only beamline program using the RDA (rotational Drickamer apparatus), which can reach lower mantle conditions and produce very high sample strains, and we will also be the only beamline using the DT25 which should also reach lower mantle conditions. We are the only deformation program using a conical slit for the cleanest diffraction patterns for stress measurements. We have the first ultrasonic system capable of measurements in lab times on the order of a second. We are the first lab program measuring elastic moduli and Q at frequencies between 1 Hz and 1 mHz (Spring8 has recently adapted our technique) into the multiple GPa range. In all of these cases, our designs have been published and other synchrotron facilities can and often do copy them. Our position in the field results from continued enhancement of experimental capabilities and is driven by the user community.

In this document, this section is followed by Description of Tools, where we describe in more depth the instruments we use to measure mechanical properties and a Description of Techniques where we describe the way in which the machines are used and the data interpreted. We devote the next section to discussing the synergy between 6BMB and other programs. The following section looks to the future, beyond 6BMB to other beamlines and what possibilities exist. We also outline how we are pursuing research questions in the community to which we can

make new contributions. In particular, we feel that we have invented extremely valuable tools that have real uses in the area of rock physics.

In the appendix, we include selected science highlights. This is the core of our program – the new science that is enabled. These one pagers illustrate recent achievements that demonstrate that 6BMB is generating paradigm-shifting results. Included are: Work that demonstrates that in-situ diffraction data provide a rich source of information about the individual plastic deformation mechanisms operating in polycrystalline materials as they deform (Burnley's group, in prep.). By using elastic plastic self-consistent (EPSC) models to interpret diffraction data they are able to measure CRSS values for important slip systems and detect the operation of other plastic accommodation mechanisms. This new ability will improve our understanding of the rheology of Earth materials. A study by Cheung et al. [2017] successfully quantifies the stress distribution in a sandstone during collapse under an externally applied stress, as revealed by X-ray diffraction. This study sheds light on compaction process involving damage, pore collapse and grain crushing, and also contradicts the assumptions of the current model used to predict yielding. Hanson and company reveal startling new evidence that fine grain aggregates are much stronger than coarse grain materials. The results have implications for the strength of the lithospheric mantle during flexure under volcanic or glacial loads, during bending of slabs at subduction zones, and after seismic events in the ductile roots of major fault zones. Dobson demonstrates that sample preparation strongly affects measurements of Q and elastic modulus. Higher pressure – up to at least 10 GPa – influences the results. This has huge implications on results that are in the literature and currently guiding our understanding of the asthenosphere. Holyoke's program recently measured the flow law for magnesite and discuss possible implications for deep focus earthquakes – note the number of undergraduate authors. Karato's program has brought deformation studies into the lower mantle. A prominent example of studies using the RDA at the beamline includes the first quantitative deformation experiments of a lower mantle material under the lower mantle conditions (Girard et al., 2016). This study showed that ferropericlase has substantially smaller creep strength than bridgmanite. While this was completed at NSLS, Karato's group is continuing this research at 6BMB and have obtained a data set on MgO suggesting that a change in the slip system occurs at pressures ~20 GPa. Raterron's program indicates that the viscosity of the Martian mantle, instead of being 10 time weaker than the Earth's due to the effect of iron, it is probably 40 times greater, thanks to deformation studies at 6BMB. Weidner's program measured ultrasonic velocities into the partially molten region of a peridotite. The results contradict current models and support a model that includes interaction of the stress wave and the phase equilibrium. Whitaker describes the new ultrasonic measurement system, first implemented at 6BMB, that reduces data collection time by about 2 orders of magnitude compared with the systems that are currently in use at most synchrotrons. The planned closure of 6BMB would disrupt and negatively impact all these user programs as well as others not described above.

The rest of the appendix includes user statistics and publications for the past several years.

2. Description of Tools

The marriage of multi-anvil tooling with the synchrotron has changed the world of high pressure deformation studies. Previously, high precision deformation measurements were limited to 300 MPa confining pressure with the lower precision 'Grigg's Rig' efforts going up to 3 GPa. With the synchrotron, measurements of strain come directly from comparison of x-ray pictures of the sample and stress measurements come from analysis of diffraction patterns, again directly from the sample. This allows the use of multi-anvil devices that have been modified to

apply the stress at the higher pressure of the multi-anvil system. Here we describe tools that are used at 6BMB; additional devices on the XPD beamline will be described below in the synergy section.

2.1. DDIA

We conceived and implemented the multi-anvil high pressure DDIA device [*Durham et al.*, 2002; *Wang et al.*, 2003] for use with synchrotron X-ray radiation [*Donald Weidner et al.*, 2005] as shown in Figure 1. This system is derived from the DIA apparatus which has been extensively used on synchrotron x-ray sources [*Shimomura*, 1985]. This apparatus forces six anvils to synchronously advance on a cubic pressure medium (Figure 1). The DDIA modification is to add hydraulic jacks to push on the upper and lower anvils. This allows the application of a non-hydrostatic stress to the entire cubic cell assembly, while at the same time, the main ram can be adjusted so as to maintain a constant pressure. A typical cell assembly is illustrated in Figure 2. The cylindrical geometry of the sample assembly includes hard pistons above and below the sample chamber that transmit the stress produced by the loading anvil to the sample. The upper and lower rams can be driven at a constant rate producing a constant strain rate from 10^{-7} to 10^{-4} s^{-1}. The stepping motors that drive the hydraulic rams can also produce sinusoidal stress fields with frequencies between 0.2 and 0.0001 Hz with a stress amplitude between 50 MPa and 5 GPa. The side anvils need to be x-ray transparent in order to measure x-ray diffraction in the horizontal plane. Cubic boron nitride and sintered diamond have both been used for this purpose.

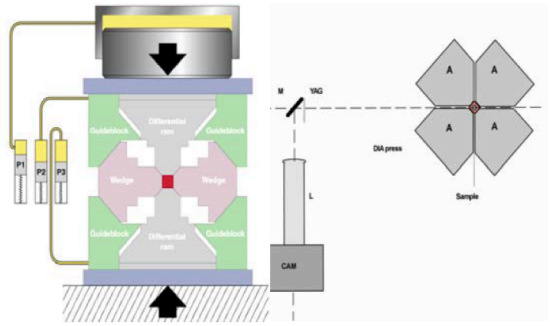

Figure 1. Left: Sketch of DDIA, a deformation device with tetragonal symmetry, in which large strain can be generated up to 10GPa and 2000K. Right: CCD camera used to take X-ray radiograph of the sample.

Pressure of 15 GPa and temperature of 2000K can be reached. Mechanical testing [*Li Li and Weidner*, 2007] can be performed on single crystal or polycrystalline samples 1-3 mm length and 1-1.5 mm diameter. Polycrystalline samples can be pre-sintered or powder which requires sintering *in situ* at high temperature. For mechanical testing, each specimen is enclosed in either metal foil of 25 micron thickness, or a graphite capsule in order to isolate the sample from the surrounding boron nitride sleeve and control the

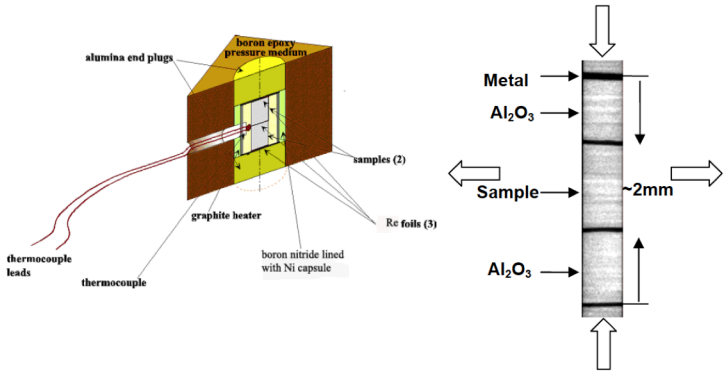

Figure 2 Left: cell assembly, right: X-ray radiograph of the sample. The arrows represent the uniaxial compression direction of the DDIA device. From the top to bottom is a Al_2O_3 rod, specimen, and a second Al_2O_3 rod separated by metal foils. The vertical direction is the axial direction.

oxidation environment. The sample ends are marked with a layer of foil. Typically the sample is used in sequence with one or two alumina reference rods that can be either sapphire (along (0001) direction) or dense alumina (~ 20 micron grain size). A boron nitride sleeve is placed between the capsule and graphite furnace for insulation. The pressure medium cube (as in Figure 2), composed of soft materials such as Boron epoxy, is typically of 6.15mm edge length. At the ends of the sample and corundum reference, crushable alumina rods of 2 mm length are placed to protect the sample from deformation during initial pressurization.

2.2. RDA

The RDA (rotational Drickamer apparatus illustrated in Figure 3) is an apparatus in which a torsion actuator (a motor + gears) is added to the Drickamer apparatus [*Yamazaki and Karato*, 2001]. In a Drickamer apparatus, a sample is squeezed between two anvils that are supported by a gasket. This support enables us to reach higher pressure than an apparatus without gasket support such as the Bridgman apparatus. A thin (typically 200-400 micron thick) ring-shaped sample is deformed by torsion. Two disc heaters made of TiC + diamond mixture provide heat to increase sample temperature. Pressure and temperature are measured using the equation of state of calibrant materials. After reaching high P and T, a torsion actuator (motor + gears) is used to perform torsion tests. Since the deformation geometry is torsional, we can conduct deformation experiments to large strain. The maximum strain we have reached was ~300 % shear.

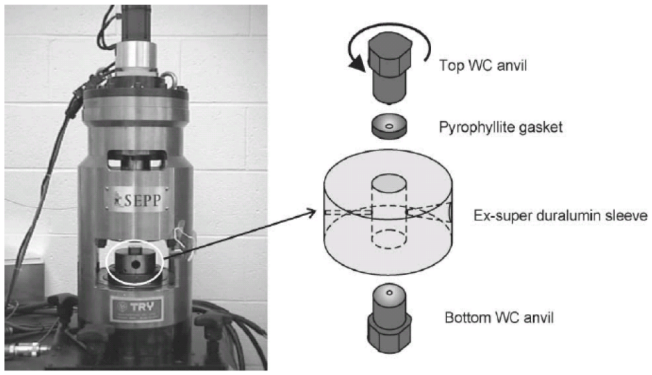

Figure 3. A rotational Drickamer apparatus for rheology and deformation microstructure studies under high P and T.

During a torsion test, we monitor the geometry of a strain marker (thin foil of heavy metal) to determine strain (rate), and observe diffracted x-rays using detectors located at various angles with respect to the sample load. Stress on a sample is calculated from the x-ray diffraction data.

This apparatus has been operated up to P=28 GPa and T=2100 K. Samples investigated include olivine, wadsleyite, ringwoodite, bridgmanite + ferropericlase.

3. Description of Techniques

3.1. Imaging the Sample with Strain Markers

As indicated above, both the DDIA and RDA utilize x-ray radiographs to measure sample strain. A powerful and non-divergent synchrotron x-ray beam, larger than the dimension of the sample, is important for making these measurements. By using high Z metal foils (such as Pt, Ni, Au, Re, etc.) that strongly absorb X-rays, and produce sharp edges in the images, strain can be analyzed. For the DDIA the strain comes from observing the change in the distance between metal foils at the top and bottom of the sample. If the experiment also needs to monitor the diameter of the sample, then a metal foil is placed around the sample and 4 x-ray transparent anvils are used in the horizontal plane instead of tungsten carbide [*D. Weidner and Li*, 2015].

The image itself is obtained from a thin YAG single crystal, which gives off visible light when bombarded by x-rays. The image is magnified and recorded by a digital camera. A DDIA sample image is shown in Figure 2. Strain data, is used in several different ways. For ultrasonic experiments, sample length can be defined from the images with an accuracy of about 1 micron. In steady state experiments, the slope of the strain – time curve, defines strain rate. For sine pump experiments (described below) sample strain is the primary measurement. Axial strain measured during sinusoidal oscillations of the load are illustrated in Figure 4. Images are taken during the forced oscillation with time. Usually 20 images per period are enough to fit a sinusoidal strain curve. This method provides a precision of fractions of 10^{-4} for a 1 mm sample [*Li Li et al.*, 2003].

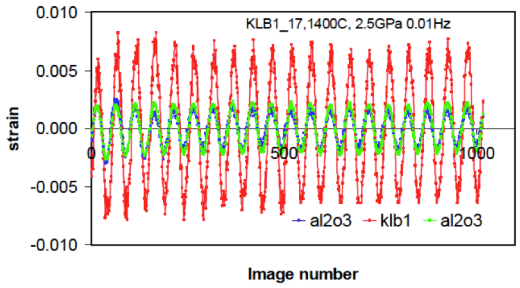

Figure 4. Sinusoidal strain-time curve. The strain is derived from sample length measured from images as in Figure 2. Each cycle has 20 frames of images.

3.2 Stress Measurements

Stress is considered a combination of pressure and the deviatoric stress tensor. Pressure is determined by the average change in lattice spacing. Deviatoric stress exists and can be measured at two different scales; macroscopic stress which is the average of the deviatoric stress across the entire sample and microscopic stresses which are the local stress states inside an aggregate. There are three types of observations that we can utilize to quantify the deviatoric stress in the sample, the choice depending on the particular goal of the experiment.

3.2.1 Peak Position

A uniaxial stress will introduce elastic strains in the sample. The strain parallel to the axis of compression will generally be larger than the strain perpendicular. The material's elastic moduli, through Hooke's law, quantitatively define the relationship between these strains and the imposed stresses. X-rays sample the distance between lattice planes (called d-spacing) whose normals are parallel to the diffraction vector, which is the bisector between the incident x-ray and the detector. The d-spacings reflect elastic strain and are insensitive to plastic strain. Figure 5 illustrates a Debye ring that would be observed from a powder sample in a stress field using a monochromatic x-ray beam and an area detector. The d-spacing is related to the distance from the center of the image to the Debye ring through Bragg's law ($n\lambda=2d\sin\theta$). For the angle $\Psi=0°$, the d-spacing observed comes from grains with that set of lattice planes oriented nearly parallel to the x_1 direction. For $\Psi=90°$, the x-rays are sampling grains with that lattice plane aligned parallel to the x_2 direction. The strains deduced from these measurements compared with ambient conditions, are related to the stresses by:

$$\varepsilon_{ij} = \sum_{k=1}^{3}\sum_{l=1}^{3} s_{ijkl}\sigma_{kl} \qquad (1)$$

where **s** is the elastic compliance tensor.

A strategy for measuring stress comes from mapping out the d-spacing as a function of Ψ. This can be done with either monochromatic x-rays or with white x-rays. In the case of white x-rays, spectra need to be collected for different values of Ψ through collimators that fix the two-theta value. A conical slit system [*Li Li et al*., 2004b] is used for this purpose as illustrated in Figure 6. The slit system itself is created by two concentric circular slits that define a cone whose angle is the desired diffraction angle (we typically use 6.5°). Solid-state detectors with energy discrimination are placed at specific values of Ψ behind the slit system. Each detector is calibrated independently. Lattice spacings are used as illustrated above to define the differential stress. The advantage of this system is that the diffracted signal is collimated by the two circular slits, limiting the volume of material along the path of the x-ray beam that contributes to the detected x-rays. In general, in our system, we do not obtain diffraction signals from the material outside of the sample, including sleeves, furnace, and pressure media. This is extremely useful, and at some times essential, to accomplish the goals of the experiment. Realizable precision for differential stress is 10 MPa [*D Weidner, J. et al*., 2010]. To our knowledge, only the Jeep beamline at the Diamond synchrotron in Oxford uses a similar slit system.

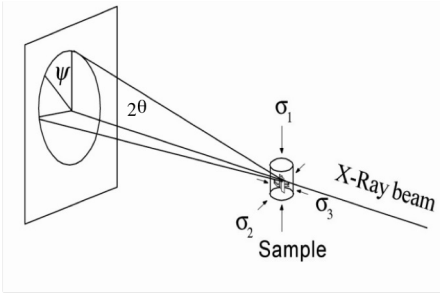

Figure 5. X-ray diffraction geometry. The stress field of the sample is illustrated by σ. In the DDIA configuration $\sigma_2 = \sigma_3$.

This technique for measuring stress is now fairly standard through out the high pressure community. The data from different lattice planes can be averaged together to estimate the macroscopic stress or the behavior of the individual lattice planes can be matched with elastic plastic self consistent models in order to derive details of deformation mechanisms operating within the sample and yield a more refined estimates of the macroscopic stress[*Burnley*, 2015].

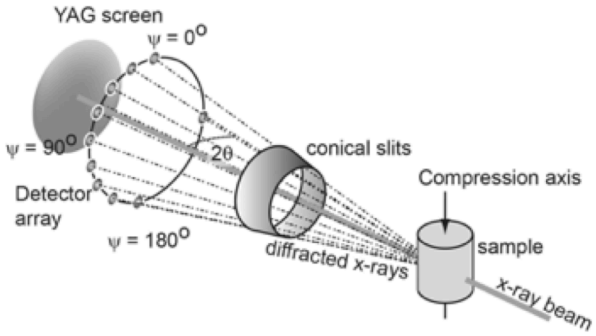

Figure 6. Schematic of the conical slit detections system. 2 circles for the cone, the sample sits at the point and the x-ray beam goes through the point. 10 detectors sit in a circular array behind the slits at the same two theta.

3.2.2 Peak Width

When the stress field in the sample is relatively uniform as it is for a fully dense polycrystal under uniaxial compression, then the diffraction peaks reflect values that are a function of Ψ as in the above discussion. If, however, the stress field is highly non-uniform, as in the case of compressing an unconsolidated powder, where deviatoric stress arise at grain contacts, the diffraction peaks broaden. We developed the use of peak broadening as a metric for the magnitude of the deviatoric stress [*D. J. Weidner*, 1998; *Donald J. Weidner et al.*, 1994a; b; *D. J. Weidner et al.*, 1994c; *D.J. Weidner et al.*, 1996]. This technique has been used to measure

the strength of diamond [*Donald J. Weidner et al.*, 1994b; *Yu et al.*, 2012] and was recently used to measure the local stress field in the collapse of sandstone as summarized in the Research Highlights by Cheung.

3.2.3 Stress Proxy

The length of the alumina rod can be used as a stress proxy as is typical in seismic attenuation measurements [*Jackson* 2007]. Assuming that the alumina is elastic in the region of study, the stress is estimated from the uniaxial strain times the Young's modulus. This measure of stress is very convenient for D-DIA sine pump studies (described below) where the stress field oscillates. Furthermore, the sample strain and the proxy strain are defined at exactly the same time.

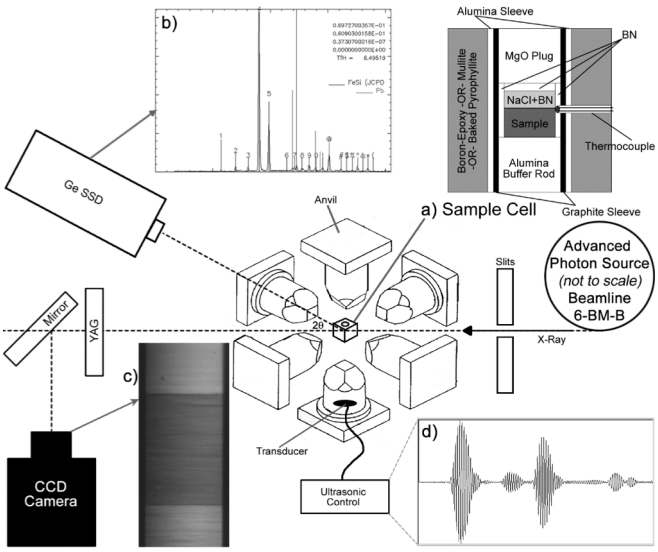

Figure 7. Outline of a typical ultrasonic experimental setup. a) Cell Assembly – Schematic diagram of the standard cell assembly used for acoustic measurement experiments. A 1μm-thick disc of Au foil is placed above and below the sample and at the bottom of the buffer rod to smooth all contact surfaces and act as a marker in the X-radiographic images. b) Sample energy dispersive X-ray diffraction pattern collected during an experiment with indexed peak positions and Pb fluorescence lines shown for reference. c) Sample X-radiographic image collected during experiment. d) Ultrasonic Interferometer allows for the collection of both P and S wave data as a function of pressure and temperature. Figure from Whitaker et al. 2017.

3.3 Ultrasonic Velocities

The development of the imaging techniques discussed previously opened a new field of study of the elastic properties of materials at high pressures and temperatures. While ultrasonic velocities had been used before to determine P and S wave velocities at high pressures, these results had been limited to room temperature studies, and the length of the sample had to be estimated based on known sample properties. The ability to directly measure the length of the sample as a function of pressure and temperature during the experiment allowed for a new host of experiments in which the elastic properties of various phases could be explored. The new method of coupling acoustic velocity measurements with synchrotron X-ray diffraction and imaging was pioneered by Liebermann and Li [*B S Li et al.*, 2004a] at the COMPRES-funded X17B2 facility. It is worth noting here that almost all other multi-anvil synchrotron facilities in the world have directly copied this experimental setup in adopting this technique. A schematic of these experiments and how they work is shown in Figure 7.

At our new facility at APS 6-BM-B, we vastly improved upon this technique by developing a new system (using external funds) for fast collection of acoustic wave velocity data in materials at high pressures and temperatures. This new system, dubbed DIASCoPE (Whitaker et al. 2017), is capable of collecting ultrasonic interferometry data, which used to take anywhere from thirty seconds to three minutes to collect, in one second or less, cutting this data collection time by over 1-2 orders of magnitude. The data obtained from DIASCoPE in 1 second have been shown to be as robust as those obtained in existing ultrasonic experimental systems that sum their data acquisitions over much longer time scales. This allows for both the study of transient

processes and increased statistical robustness of the data output collected over extended timescales similar to those employed by other systems.

In addition to its speed, this new system is unique in that it has been fully integrated into the beamline controls system rather than being a separate counterpart. This has allowed us to develop new software protocols for the automation and synchronization of data collection during an experiment. Combining this system with the conical slit and unique detector array at 6-BM-B allows for the monitoring of deviatoric stress on the sample during the experiment, which has not traditionally been done. In addition, these acoustic measurements can be synchronized and coupled with sinusoidal stress fields to see what effect cyclic loading may have on the elastic and anelastic properties of materials at high pressures and temperatures. Thus DIASCoPE will enable observations of how various processes affect the physical properties of materials at extreme conditions as they occur rather than focusing only on the products resulting from these processes. We see many opportunities for unique and paradigm-changing experiments utilizing this system in the months and years to come.

3.4 Steady State Flow Experiments

Steady state flow experiments require that the DDIA or the RDA generate a constant deformation rate that can be quantified as well as measurements that can yield stress. We generally use images to quantify the strain rate and diffraction with the conical slit to quantify stress. We have an automated data collection control system where images and diffraction measurements alternate. Data collection times for the diffraction data are typically 300 seconds, while images take about 1 ms. Slits open for the images and close for the diffraction. These experiments are carried out for several hours, often with sample strains in excess of 50%.

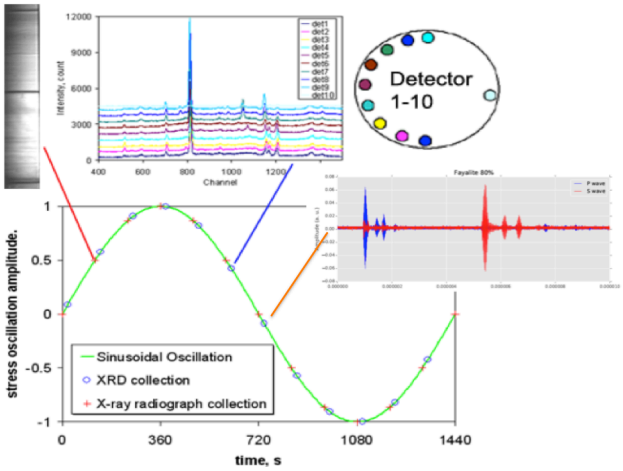

Figure 8. Synchronized X-ray diffraction, X-ray radiography, and ultrasonic P and S velocity during sinusoidal stress oscillation. Shown is for stress oscillation with a period of 1440 second. A diffraction data (shown on the top center) was collected every 120 seconds and include the energy dispersive X-ray diffraction pattern for 10 detectors. The ten detectors are distributed around a circle at a fixed two theta (arranged as shown in upper right). The patterns collected by detector 1 and detector 9 are along the unique stress axis. An X-ray radiograph is also collected every 120 second. The ultrasonic reflections include signals from both sides of the sample and take less than 1 second to gather data for both P and S waves.

In addition to quantitative flow laws, this tool can define the lattice preferred orientation produced during the flow process. The diffraction amplitude as a function of Ψ can yield this information. Users have made extensive use of this technique to refine flow laws for a multitude of geologic materials, observe changes in deformation mechanisms with pressure and temperature and study the interactions of coexisting minerals during deformation.

3.5 Sine Pump

We have developed a new

protocol for data collection that we call 'sine pump'. The differential rams are driven in a sinusoidal fashion with data collected at fixed angles of the sine function. Figure 8 illustrates the time line in this data protocol and the data types that can be taken. The images are used to define strain, the diffraction defines stress and the ultrasonics define P and S velocities. The user predefines the amplitude and period of the sine function as well as the angles where the specific data will be collected. We have successfully collected data with periods as short as 5 seconds and as long as 5 hours. At low amplitudes, Young's modulus and Q can be measured [*Li Li and Weidner*, 2007] or amplitudes can be large enough to induce to induce plastic flow and measure lattice preferred orientations [*L. Li and Weidner*, 2015] and potentially plastic flow laws.

3.6 General Purpose

The beamline at 6BMB can serve as a multi-anvil beamline for studying a wide range of phenomena including phase transformations, and equations of state, that are studied with multi-anvil systems that use either x-ray diffraction or x-ray imaging as long as they are compatible with the pressure and temperature range of the system. The range of pressure that is accessible is restricted by the anvil truncation. We have been pushing to lower pressures, with studies that concentrate on a few hundred MPa, and we are developing anvils with small truncations to reach up to 15 GPa.

4. Synergy

As mentioned above 6BMB is part of a larger program that includes the XPD beamline at the NSLS II. These two beamlines offer complementary capabilities with some experiments being better served at one site than the other. For example, XPD will offer the higher pressure deformation device, while 6BMB offers white diffraction with the conical slit.

4.1 XPD

We are building an endstation in hutch D of the XPD beamline at the NSLS II. This is a damping wiggler source that routinely works as a monochromatic beamline at 52 or 70 kev. This high energy will be advantageous since it is very penetrative and the diffraction signal will cover a small two-theta region, yielding more diffraction rings in a limited two-theta aperture. In this hutch, we will place the first DT25 ever on a synchrotron. We use a Perkin-Elmer (1621 CN3 EHS) flat panel detector, CsI phosphor directly deposited on amorphous silicon, 2048x2048 pixels with 200x200 micrometer pixel size, 15 frames per second readout at 2048x2048, and 30 fps at 1024x1024.

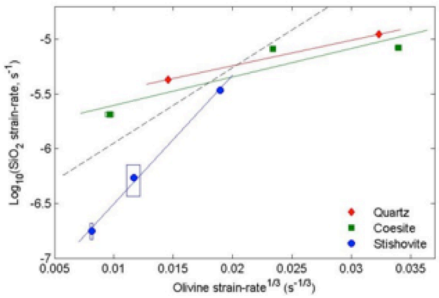

Figure 9. SiO_2 strain-rate against olivine strain-rate to ⅓ power, which is proportional to stress at constant temperature for $n_{ol} = 3$. Solid lines are example fits to the data. In both plots, the rectangles delimit the strain-rates' standard errors and the black dashed line are the 1:1 equal strain-rate line.

The DT25 is a larger version of the DT10. These instruments have Kawai-type guideblocks which generally delivers 2 to 5 time more pressure than does the DIA for a similar sample volume. In Kawai-type (6-8) devices eight cubic anvils are used to compress the sample assembly. In the DT10 and DT25 two of the eight cubes which sit along the split-cylinder axis have been replaced by hexagonal cross section anvils. Driving these hexagonal-anvils with secondary differential actuators incorporated into the

load frame enables the 6-8 multi-anvil apparatus to be used for controlled strain-rate deformation experiments to high strains. Testing of the design, both with and without synchrotron-X-rays, has demonstrated the DT10 is capable of deforming 1–2 mm long samples to over 55% strain at high temperatures and pressures.

Weidner and Dobson designed the DT system several years ago [*S. A. Hunt et al.*, 2014]. While the DT25 has not been tested, both Weidner's and Dobson's programs have had several years of experience with the DT10. Prior to the closing of the NSLS, the DT10 was commissioned on the side station beamline X17B2ss. In the commissioning experiments SiO_2 polymorphs quartz, coesite and stishovite were deformed to high strain concurrently with olivine [*Simon A. Hunt et al.*, 2017]. The strengths of the principle phases of SiO_2 (quartz, coesite and stishovite) were determined from these experiments. Quartz and coesite deformed by Harper-dorn creep and had very similar strength (Figure 9). Stishovite in contrast deformed by power-law creep or grain-boundary sliding and is significantly stronger than the lower pressure polymorphs. We interpret these results to imply that stishovite is a strong phase in the subducting slab. Moreover, the biggest change in properties between stishovite and the other SiO_2 phases is the coordination of silicon in the crystal structure. We conclude that greater strength of stishovite arises from the Si-coordination change. The NSLS was closed before further studies could be undertaken at the NSLS. However, bridgmanite has been deformed under lower mantle conditions to high strains, using an almost identical copy of the DT10 at University College London (London, UK).

The DT25 has 25 mm instead of 10 mm anvils. It will be driven by a 1000 ton press and include two 250 ton differential jacks driving the upper and lower anvils. While we have not used this guideblock yet, we have used the 1000 ton press for several years at the NSLS. We have explored several strategies for transparent cubes. The current preference is to purchase sintered diamond anvil 25 mm cubes that are commercially available for only about 4 times the cost of tungsten carbide. We have used such assemblies with 3 mm truncations for several runs at a 500-ton load in the Stony Brook Sumitomo press with no failures of the sintered diamond anvils to date.

The DT25 can serve as a hydrostatic device as well as a deformation device. Ultrasonic experiments will be possible in this machine as well as the standard phase equilibrium or equation of state study. We anticipate that the DT25 will be the highest pressure multi-anvil uniaxial deformation device. It should compete with the RDA for maximum pressure.

In addition, a DDIA module (on loan from UC Riverside) is available and can easily and quickly replace the DT25.

4.2 GSECARS

Our multi-anvil program has a long history of synergy as well as competition with GSECARS. Weidner was the design team leader of the multi-anvil program at GSECARS when GSECARS began. We brought our the design of Kawai style guideblock and, later, the DDIA to GSECARS. When we upgraded our electronic system, we imported Mark River's EPICS system for driving motors and for data visualization and storage. Yanbin Wang was a student at Stony Brook and was a staff member when he went to GSECARS. Since then, the systems have evolved somewhat independently, but with discussion and interaction. We share the Rheology Grand Challenge grant with Yanbin even today. Since moving to 6BMB, Mark Rivers has been extremely generous with his time to help trouble shoot several difficult situations and often to provide an equipment loan for items that break down in use. This is particularly important since our technical support personnel are at Stony Brook. Right now, I believe, that we have slightly

more beamtime than does the GSECARS multi-anvil program, but we have had more in the past and expect to increase our beamtime when XPD comes on line. We both operate with two beamline scientists, while GSECARS also has a post doc. We estimate that our publication record over the past five years is about 2 to 3 times greater than the multi-anvil GSECARS program.

We feel that it would be useful to strengthen the ties with GSECARS. One suggestion would be for us to share the cost of a technical support individual. A mechanical oriented person would be our first preference to help with high pressure support (not included in the current budget).

5. Future

Beamline 6BMB was designated as a 'white beam dark period' replacement for large volume high pressure research at the close of the NSLS. This was negotiated among management of APS, NSLS, COMPRES, and JPSI (Joint Photon Science Institute of BNL and Stony Brook). Along with multi-anvil research, X17 served a number of programs that need to restrict the diffraction volume along the beam. Battery research was a big group among these as they are studying the spatial distribution of chemical reactions in a discharging battery. While a bending magnet has about a factor of 5 lower flux than X17, the flux density at 6BMB is about a factor of 3 to 4 greater than at most of the other bending magnet beamlines since the hutch is so close to the source. Otherwise, beam characteristics at 6BMB are very similar to X17. Furthermore, the system parameters at APS are compatible with the hardware and software of the multi-anvil program. This allowed a fairly quick setup.

The future location of the white beam multi-anvil program is an important issue that we have been pursuing. Coupled with this is an interest in the user community in broadening the scientific scope of the program as well as exploring new technical capabilities that are under development in the materials science community. About two and a half years ago, New York State announced that it was donating $25M to build a superconducting wiggler beamline at the NSLS II. Two months ago, the final papers were signed, and this month, the first check is due to arrive at BNL. Construction will be about 4 – 5 years. The new beamline, HEX, will consist of 2 simultaneously operating white beams (that can be monochromatic by choice of the researcher) and one monochromatic beamline. HEX will have one of its white beam end stations outside the ring building in series with another white beam hutch inside. The other white beam and the mono beam station will be inside the ring building. The outside hutch will boast a beam that is 25 mm in the vertical dimension and larger in the horizontal. HEX will specialize in very high resolution imaging with various high contrast techniques in use, along with diffraction including multi-grain diffraction.

We feel that HEX is the ideal location for the current multi-anvil program. The flux will be more than an order of magnitude greater than at X17 and the imaging capabilities open new possibilities for future research. We are struck by the size of the beam as it will open opportunities for rock physics that did not exist before. Sample size in rock physics has always been considerably larger than that of the typical mineral physics needs. The new beam size with the concentration on imaging should be very useful to that community. We have been building connections over the past few years with members of that community including executive committee members of DEFORM and believe that there is enthusiasm in that community to join in this effort. The combination of beam size and flux is will be unique in the world and even more so with the upgrades at APS, ESRF, and Spring8 to bring more coherent beams that will be even smaller than they are now.

Our plan going forward is bring together the user community to define the scientific questions that can be addressed, and collaboratively seek funding to design and test instrumentation while the beamline is under construction. In the near term, we plan to hold a workshop to bring the various communities together with NSLS staff outlining science needs and technical answers. We have conducted a small version of this with telephone meetings, but need to broaden this to a larger scale. The goal is to design equipment for specific needs. For example, it may not be optimal to use a 1000 ton press for 100MPa experiments. Constraints from the x-ray experiment will also be considered. For example, tomographic images need 360^{o} access. This might be a lot easier at 100MPa than at 30 GPa. As ideas develop, we plan to run pilot studies with 6BMB to test the concepts. This effort would benefit with the addition of a post doc at 6BMB (for which we will seek independent funding). By using the next 5 years to develop and build the ideal equipment for the specific needs, we will be ready to implement the new experimental program when HEX opens We would go to the MRI program or some equivalent to make the final apparatus.

Now that the agreement with New York State has been finalized, the management at NSLS II is in a better place to have concrete discussions regarding the usage of HEX. We have a long relationship with the NSLS II management. In 2010, we submitted a proposal to build a superconducting wiggler beamline dedicated to high pressure research at the NSLS II. This proposal was with the understanding that DOE would fund the beamline. It was reviewed by NSLS II management, the SAC, by an outside review panel, and was accepted. When it became apparent that the DOE only had funds to build a very small number of beam lines, most of the successful proposals were dismissed unless they could also generate the funds. The high energy, white beam proposals have generally become swept up into this new HEX beamline. Some of the management diagrams of the HEX floor space already have a large hydraulic press indicated. Now, we need to identify financial needs that NSLS II will have in building and/or operating. It is highly likely that we will gain commitments to beam time if we can provide funding for some of the beamline's essential needs.

Weidner recently spoke with Dr. Z. Zhong, the senior NSLS scientist at X17 and the recent designer of HEX, who will be the person in charge of construction of HEX. Zhong reiterated that HEX was designed with multi-anvil high pressure work in mind, and that he felt that ample beam time would be available for our program. He further assures us that he will work with us over the coming few years to design high pressure experimental apparatus that will enable advances in our experimental program.

It has been suggested that an alternative to going to HEX is to stabilize the 6BMB program at APS. Even though 6BMB has 3 to 4 times flux density than most beamlines because of its closeness to the source, more flux would be very useful. As the Facilities Committee indicated, a mirror can increase the flux density by an order of magnitude. Of course this comes with a decrease of the vertical dimension of the beam by at least an order of magnitude. Thus, most imaging would require that the mirror be inserted and removed as one switched between diffraction and imaging. The beam will move up or down with this action. It is not clear whether or not this can be automated and kept to a time loss of no more than a few seconds. In addition, we need to have the range of motion of the press to make the change as the mirror is removed.

6. Impact of 6BMB closure on the user community

The planned closure of 6BMB would have large negative consequences on the current user community using 6BMB as well as at XPD when it opens. The loss of white beam

capability with our conical slit system would stop all work in the RDA until that capability could be recreated elsewhere. The funding to recreate that capability has not to date been identified. It has been suggested that users of the DDIA could migrate to GSECARS but GSECARS beamlines are already over-subscribed, and our program would more than double the existing multi-anvil program at GSECARS. Therefore, the amount of beamtime for the deformation community would be diminished and the existing user base at GSECARS would also see their access to beam time cut. Independent of how it is distributed, the high pressure community would see a decrease in 3300 hrs/year of synchrotron time. When XPD comes on-line some DDIA users will be able to work there, but at the cost of developing and exploiting the new DT25. However, the loss of the second beamline scientist will negatively impact XPD user operations as well. Finally there will be tremendous inefficiency for all 6BMB users who need to develop new data collection and analysis protocols as they adjust their research programs to different instrumentation, different data streams, and decreased access to beam time. Thus the community would be spending its energy on recuperation efforts rather than advancing the cutting edge of in-situ deformation studies.

7. References

Burnley, P. C. (2015), Elastic Plastic Self Consistent (EPSC) Modeling of Plastic Deformation in Fayalite Olivine, *American Mineralogist*, *100*, 1424 – 1433, doi:10.2138/.

Durham, W. B., D. J. Weidner, S.-i. Karato, and Y. Wang (2002), New developments in deformation experiments at high pressure, in *Plastic Deformation of Minerals and Rocks*, edited by S.-i. Karato and H.-R. Wenk, pp. 21-49, Mineralogical Society of America, San Francisco.

Hunt, S. A., D. J. Weidner, R. J. McCormack, M. L. Whitaker, E. Bailey, L. Li, M. T. Vaughan, and D. P. Dobson (2014), Deformation T-Cup: A new multi-anvil apparatus for controlled strain-rate deformation experiments at pressures above 18 GPa, *Review of Scientific Instruments*, *85*(8), doi:10.1063/1.4891338.

Hunt, S. A., M. L. Whitaker, E. Bailey, E. Mariani, C. Stan, and D. P. Dobson (2017), The effect of Si-coordination on the rheology of SiO2 polymorphs, *Geophys. Res. Lett.*, in preparation.

Jackson , I. (2007), Physical Origins of Anelasticity & Attenuation in Rock, in *Treatise on Geophysics*, edited by G. Schubert, Elsevier, Amsterdam.

Li, B. S., J. Kung, and R. C. Liebermann (2004a), Modem techniques in measuring elasticity of Earth materials at high pressure and high temperature using ultrasonic interferometry in conjunction with synchrotron X-radiation in multi-anvil apparatus, *Physics of the Earth and Planetary Interiors*, *143*, 559-574, doi:10.1016/j.pepi.2003.09.020.

Li, L., P. Raterron, D. Weidner, and J. Chen (2003), Olivine Flow Mechanisms at 8 GPa, *Physics of the Earth and Planetary Interior*, *138*(2), 113-129.

Li, L., D. Weidner, P. Raterron, J. Chen, and M. Vaughan (2004b), Stress measurements of deforming olivine at high pressure, *Physics of the Earth and Planetary Interior*, *143-144*, 357-367.

Li, L., and D. J. Weidner (2007), Energy dissipation of materials at high pressure and high temperature *Review of Scientific Instruments*, *78*(1), DOI: 10.1063/1061.2735587.

Li, L., and D. J. Weidner (2015), In situ analysis of texture development from sinusoidal stress at high pressure and temperature, *Review of Scientific Instruments*, *86*(12), doi:10.1063/1.4937398.

Shimomura, O., Yamaoka S., Yagi T., Wakatsuki M., Tsuji K., Kawamura H., Hamaya N., Fukuoga O., Aoki K., and Akimoto S. (1985), Multi-anvil type X-ray system for synchrotron radiation, Terra Scientific Publishing.

Wang, Y., W. Durham, I. C. Getting, and D. Weidner (2003), The deformation-DIA: A new apparatus for high temperature triaxial deformation to pressure up to 15 GPa, *Rev. Sci. Instrum.*, *74*, 3002-3011.

Weidner, D., J. , M. Vaughan, T., , L. Wang, H. Long, L. Li, N. Dixon, and W. Durham, B. (2010), Precise Stress Measurements with White Synchrotron X-rays, *Review of Scientific Instruments*, *81*, 013903.

Weidner, D., and L. Li (2015), Kinetics of Melting in Peridotite from Volume Strain Measurements, *Physics of the Earth and Planetary Interior*, *246*, 25-30.

Weidner, D., L. Li, W. Durham, and J. Chen (2005), High-temperature plasticity measurements using sychrotron X-rays, in *High-pressure technology for geophysical applications*, edited by J. Chen, Y. Wang, T. S. Duffy, G. Shen and L. F. Dobrzhinetskaya, pp. 123-136, ELSEVIER Inc., San diego.

Weidner, D. J. (1998), Rheological studies at high pressure, *Reviews in Mineralogy, ultrahigh-pressure mineralogy*, *37*, 493-522.

Weidner, D. J., Y. Wang, and M. T. Vaughan (1994a), Deviatoric stress measurements at high pressure and temperature, in *High-Pressure Science and Technology (Proceedings of the 1993 AIRAPT Conference)*, edited by S. C. Schmidt, J. W. Shaner, G. A. Samara and M. Ross, pp. pp. 1025-1028.

Weidner, D. J., Y. Wang, and M. T. Vaughan (1994b), Strength of diamond, *Science*, *266*, 419-422.

Weidner, D. J., Y. Wang, and M. T. Vaughan (1994c), Yield strength at high pressure and temperature, *Geophy Res Lett.*, *21*, 753-756.

Weidner, D. J., Y. B. Wang, G. Chen, and J. Ando (1996), Rheology measurements at high pressure and temperature, *Program and Abstracts, U.S.-Japan Seminar, High Pressure-Temperature Research: Properties of Earth and Planetary Materials*, *80*.

Yamazaki, D., and S. Karato (2001), High-pressure rotational deformation apparatus to 15 GPa, *Rev. Sci. Instrum.*, *72*, 4207-4211.

Yu, X., P. Raterron, J. Zhang, Z. Lin, L. Wang, and Y. Zhaob (2012), Constitutive Law and Flow Mechanism in Diamond Deformation, *Scientific Reports*, *2*.

Appendix I Research Highlights

Using in-situ Diffraction and Elastic Plastic Self-Consistent Models to Quantify Plastic Deformation Mechanisms

Pamela C. Burnley and Shirin Kaboli, University of Nevada, Las Vegas

In-situ diffraction data provides a rich source of information about the individual plastic deformation mechanisms operating in polycrystalline materials as they deform. The challenge is to determine how to best extract this information from the raw diffraction data. We have been using elastic plastic self-consistent (EPSC) models to interpret diffraction data in terms of the deformation mechanisms operating

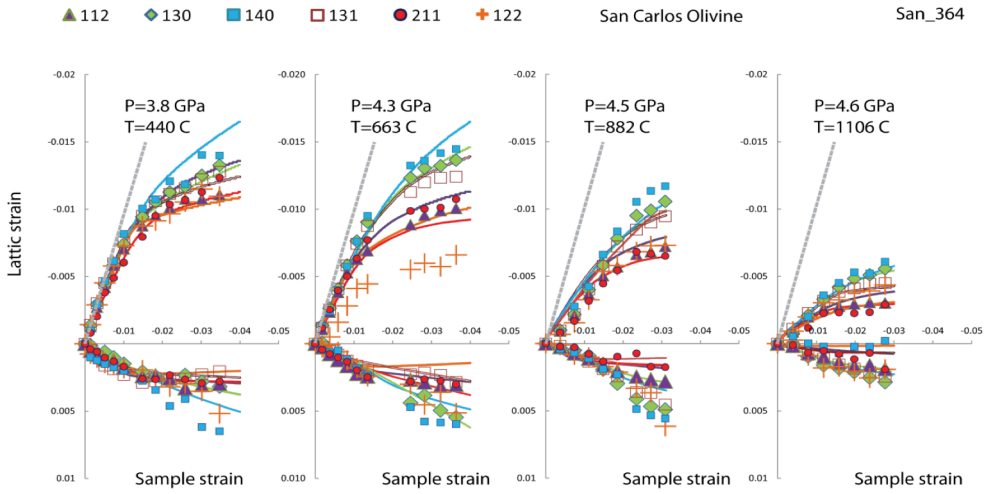

Figure 2: *Lattice strain vs sample strain for deformation experiments conducted on San Carlos Olivine at 5 x 10-6/sec. The solid lines are the EPSC models and the symbols are the diffraction data. The dashed grey line depicts the self-consistent elastic slope.*

in the sample. We conducted a suite of low strain experiments at ~5 x 10^{-6}/sec at temperatures ranging from 440 C to 1100 C in the D-DIA apparatus at APS 6BMB. For each experiment we fit the diffraction data using EPSC models that included an isotropic deformation mechanism that work hardens rapidly, [001] slip, and kinkband formation. The models closely reproduce the diffraction data (Figure 1) and yield estimates for the CRSS of [001] slip that are comparable to those found in the literature (Figure 2). The isotropic deformation mechanism allows us to model the data's deviation from the self-consistent value of the Young's modulus (Figure 1 -grey lines). Although we have not confirmed the exact nature of this deformation mechanism the models provide us with quantification that can be used to compare with proposed mechanisms.

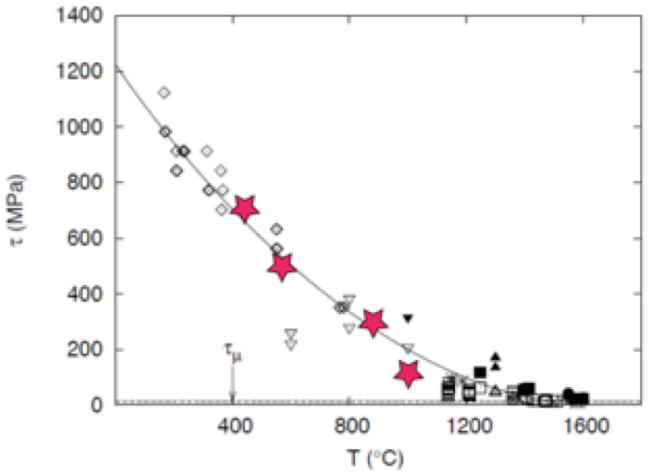

Figure 1: *CRSS for [100] slip in olivine from Durink et al Am. Min.v. 92, 2007. Red stars are values determined in this study from EPSC models*

Stress distribution during cold compression of a quartz aggregate using synchrotron X-ray diffraction: Observed yielding, damage and grain crushing [*Cheung et al.*, 2017]

Cecilia Cheung, U Wisconsin

Compaction in porous rock is of fundamental importance to reservoir and geotechnical engineering. Any natural phenomena or artificial geological (e.g., oil and gas extraction) application that reduces pore pressure is likely to cause an increase in the effective stress. Such an increase in effective stress may be sufficient to cause inelastic deformation of the reservoir rock. In geomaterial, stress is likely to concentrate at grain-to-grain contacts and vanish where grains are bounded by open porosity. Therefore, internal stress is likely to vary significantly from point to point in such an aggregate, and hence, it is important to understand and quantify the stress distribution with respect to the externally applied stress. Our samples were probed with synchrotron X-ray diffraction as they were compressed in a multianvil deformation apparatus at ***X17B2*** and ***6BM*** at room temperature from low pressure (tens of megapascal) to pressures of a few gigapascal. Stress was indirectly by using the atomic lattice spacing within grains, as revealed by X-ray diffraction, as a measure of local elastic strain, on samples of a quartz aggregate and a novaculite (as end-members of the spectrum of quartz-rich geo-materials).

In our quartz aggregate, the diffraction peaks broaden asymmetrically at low pressure (tens of megapascal), suggesting that open pores are still a dominant characteristic of grain boundaries. In contrast, a reference sample of novaculite (a highly dense quartz polycrystal) showed virtually no peak broadening with increasing pressure. In the quartz aggregate, a significant deviation was observed in the pressure-volume curves in the range of P = 400–600 MPa. We suggested that this marks the onset of grain crushing (generally denoted as P* in the rock mechanic literature), which is commonly reported to occur in sandstones at pressures of this order, in general agreement with a Hertzian analysis of fracturing at grain contacts. In this region, the sample compresses significantly with little increase in pressure. Furthermore, at the time of collapse, we found that the differential microscopic stress is about 1000 MPa. These values are about an order of magnitude lower than those predicted by a model based on Hertzian fracture mechanics.

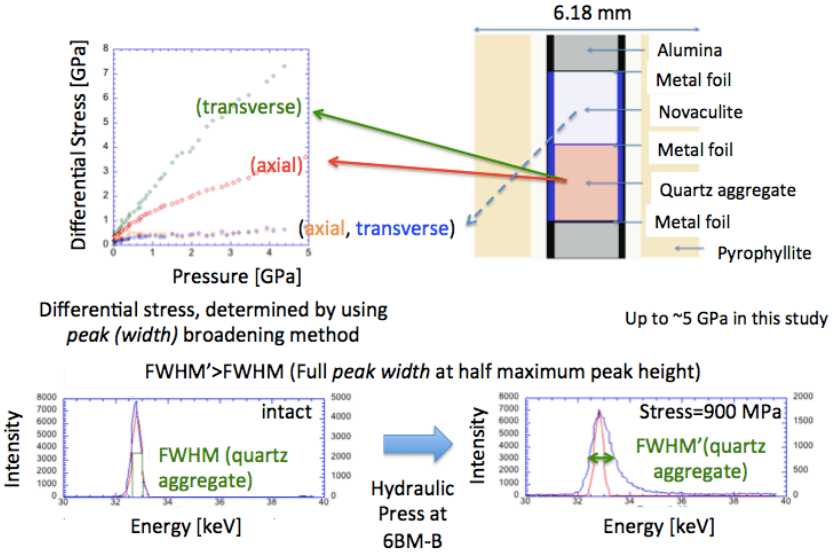

The grain-size dependence of yield strength during low-temperature plasticity of olivine: Evidence for weak lithospheric mantle

Lars N. Hansen, Kathryn M. Kumamoto, Christopher A. Thom, David Wallis, David L. Goldsby, William B. Durham, David L. Kohlstedt

A set of experiments specifically designed to investigate an hypothesized *inverse* relationship between grain size and low-T strength of olivine was initiated with exploratory experiments in the 2017-1 trimester at 6BM-B (APS) and continued as its own GUP for 2017-2. The results strongly signal confirmation of the hypothesis. Concurrent EBSD mapping and slip system models are aimed at providing a consistent physical mechanism for the effect. The results have implications for the strength of the lithospheric mantle during flexure under volcanic or glacial loads, during bending of slabs at subduction zones, and after seismic events in the ductile roots of major fault zones. Furthermore they could explain the inconsistencies among previous studies of lithospheric strength.

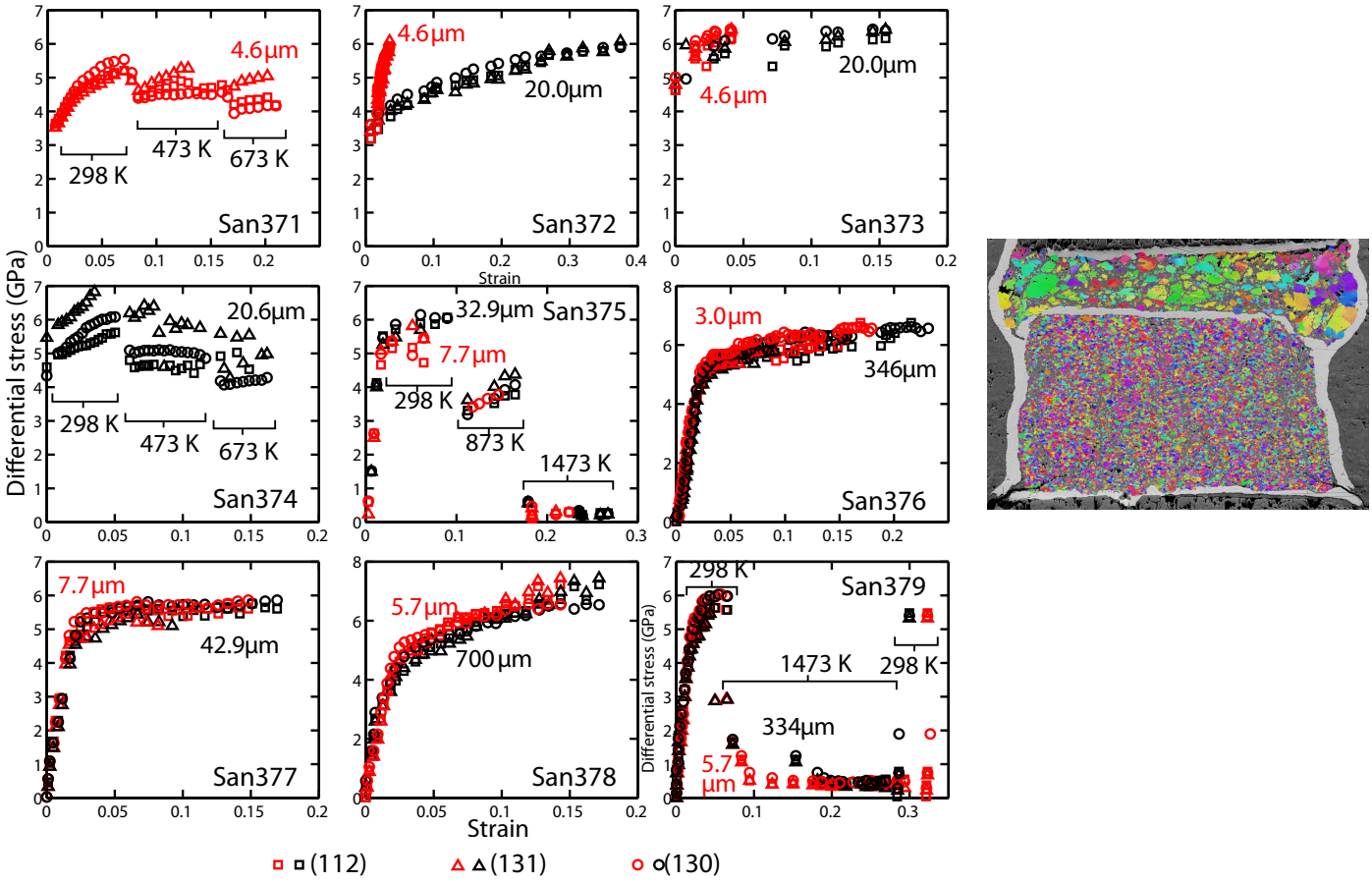

Figure 1. Stress-strain creep curves for stacked olivine samples of contrasting grain size and deformed in the D-DIA at 6BM-B at APS. Symbol shapes refer to (hkl) diffraction condition used to determine stress. Tests were at room T or as indicated. Red refers to the finer grain sample in the stack, black to the coarser. Stresses are generally the same in both samples since they are stacked on top of one another; what differs in fine vs. coarse-grained (red vs black) is strain rate, with the weaker piece strain (almost always black) extending farther along the horizontal axis than the red. Inset shows EBSD map of post-test polished section though the stack (colors indicate crystallographic orientation).

The effect of sintering pressure on the anelastic properties of pyrope
In preparation for PNAS.

Dobson DP[1], Hunt SA[1], Schardong L[1], Thomson AR[1], Ezad IS[1], Bailey, E[1], Walker AM[2], Lord, OT[3], Marquardt, K[4], Melai, C[4], Whitaker, ML[5] and Weidner, DJ[5]

Much of our understanding of the interior of the Earth comes from interpreting the behaviour of seismic waves. Grain-boundaries form a finite volume fraction of the Earth's mantle but their effects on the seismic properties of the mantle are not fully understood. Grain-boundaries undergo a fundamental change in their properties between ambient and 'high' pressure. The changes are attested to by, among other effects, the disappearance of the 'grain-boundary' component in electrical conductivity measurements at high pressure and the increase of microhardness with sintering pressure in both pure metals (Edalati & Horita, 2010, Mat. Trans., 51, 1051) and polycrystalline diamond-SiC composites (Osipov et al 2004, Mat. Res., 7, 335). These phenomena imply that grain-boundaries properties become more "lattice-like" with increasing pressure.

To test the potential consequences of this for the Earth, we performed anelasticity measurements on pyrope samples sintered at pressures between 4 and 15 GPa. All recovered samples had a similar grain size of ~2µm but the 15 GPa samples were much lighter in colour than those sintered at lower pressures. All samples were deformed by small sinusoidal strains under identical conditions of ~3 GPa, 500 to 1300°C and at periods between 10 and 1000s. At <900 °C and short periods the effective Young's modulus is the same as that predicted using the elastic constants of pyrope (Figure 1) and the quality factor (Q) is high. At higher temperatures the samples sintered at low pressure show significant reduction of the effective Young's modulus and Q, whist the samples sintered > 10 GPa maintain a high Q value

Figure 1: Effective Young's modulus (E*), at 120s period, for the 'low pressure' and 'high pressure' samples in this study. The effective Young's modulus is significantly reduced at high temperatures in the low pressure samples.

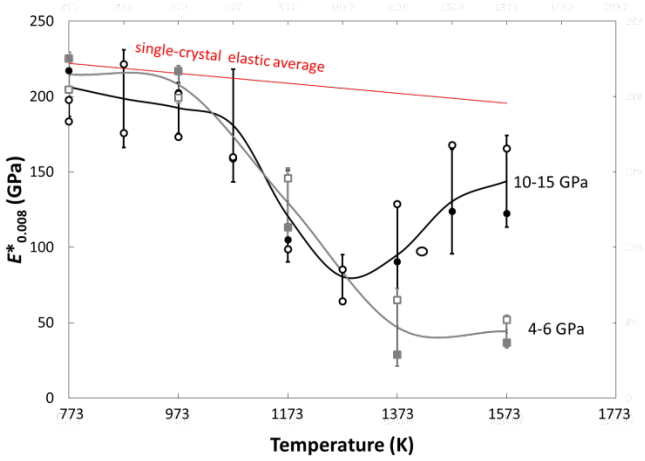

These results indicate that grain boundaries in pyrope equilibrated at high pressure can be recovered to ambient conditions but the sintering pressure strongly affects the anelastic behaviour of ceramic materials. We interpret this as a pressure-induced inhibition of the elastically accommodated grain-boundary sliding mechanism due to enhanced strength of grain boundaries created at high sintering pressures.

Grain size and pressure dependence of magnesite aggregate rheology: implications for nucleation of intermediate depth (200-400 km) deep focus earthquakes.

C. Blasko[1,*], N. Jackson[1,*], C. McDaniel[1,**], J. Millard[1,**], C. Holyoke[1], A. Kronenberg[2], P. Raterron[3], L. Tokle[3, **]

1 – University of Akron, 2 – Texas A&M University, 3 – Brown University, * - undergraduate student, ** - graduate student. This study is supported by NSF EAR-1624242 to Holyoke, Kronenberg and Raterron.

In many down-going slabs, such as the Nazca plate beneath Chile, earthquake foci are observed in two depth-related groups separated by an aseismic zone from ~200 to 400 km depth. The mechanisms commonly proposed for the earthquakes above and below the aseismic zones are serpentine dehydration and phase transitions in olivine, respectively. However, in other subducting slabs, such as the Pacific plate beneath Tonga, earthquake foci are observed continuously from the surface to the transition zone (~660 km depth). The mechanism proposed for earthquakes in this zone is the formation of ductile instabilitites due to olivine recrystallization that causes a reduction in grain size and viscosity. However, since all slabs are composed dominantly of olivine, ductile instabilities in olivine should form in all subducting slabs and there should be no aseismic zones in downgoing slabs. Another possible mechanism is strain localization in magnesite, an alteration product in found in some peridotites. Magnesite is stable to depths >700 km and is orders of magnitude weaker than olivine at all pressure and temperature conditions of subducting slabs.

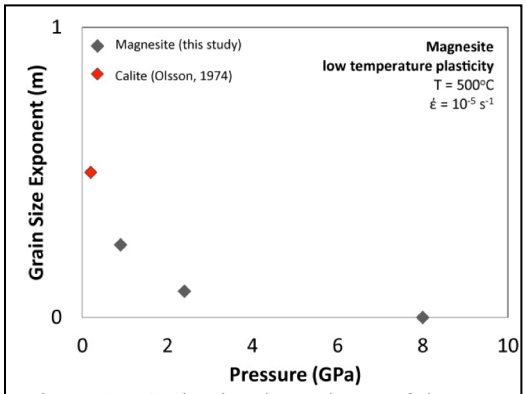

Figure 1 – Grain size dependence of the strength of magnesite decreases with increasing pressure.

In order to determine the grain size and pressure dependence of the strength of magnesite deforming by dislocation creep and low temperature plasticity, we have performed experiments using the D-DIA at beamline 6-BMB at the Advanced Photon Source at Argonne National Laboratory. Experiments were performed at temperatures from 500-900°C, pressures from 3-8 GPa and a strain rate of 10^{-5}/s.

Strengths of magnesite aggregates in experiments performed at conditions where low temperature plasticity mechanisms are dominant increase with increasing pressure. At low pressures (0.9-5 GPa), magnesite aggregates with coarser grain sizes are weaker than those with finer grain sizes. This inverse grain size-strength relationship is consistent with previous results for calcite obtained at low pressure (0.2 GPa). However, this inverse grain size-strength relationship gradually decreases as pressures increase and at 7 GPa, there is no grain size dependence to this deformation mechanism (Fig. 1). These results indicate that throughout much of its stability field the strength of magnesite is insensitive to grain size.

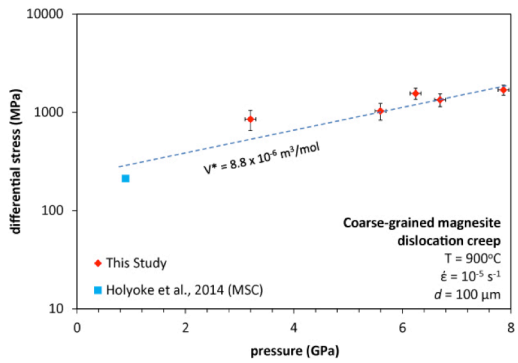

Figure 2 – The pressure dependence of magnesite deforming by dislocation creep (~9*10^{-6} m^3/mol) is similar to olivine.

Strengths of magnesite aggregates in experiments performed at conditions where dislocation creep is the dominant mechanism increase with increasing pressure, yielding an activation volume (V*) of 9*10^{-6} m^3/mol, which is very similar to that of olivine (Fig. 2). These results indicate that the high strength contrast between magnesite and olivine will not be affected by increasing depth and may cause strain localization in magnesite veins or layers in subducting slabs and, possibly, deep focus earthquakes at all depths in subducting slabs.

Studies by the Yale program at NSLS (Karato)

We use RDA (rotational Drickamer apparatus) combined with the synchrotron x-ray facility at X17B2 at NSLS to study the plastic flow behavior of materials under high-pressure and temperature conditions. We have conducted quantitative deformation experiments on two important minerals in Earth's transition zone (410 to 660 km depth). The flow laws (stress-strain rate relationship) of these minerals were investigated using the *in-situ* X-ray diffraction and x-ray radiography. These studies have provided constraints on the resistance of these minerals for plastic flow under a broad range of conditions.

In addition, we have pushed the pressure limit of quantitative studies on plastic flow in order to understand the plastic properties of minerals in the lower mantle (660-2890 km). This is the largest portion of the rocky part of this planet. By analyzing the diffracted x-ray from various portions of the sample, we realized that a substantial pressure gradient is present in the sample assembly of RDA. Consequently, we reduced the sample size to conduct deformation experiments at pressures of ~27 GPa and temperature of ~2100 K (both P and T were determined by the equations of state of two materials). Under these conditions, dominant minerals are $(Mg,Fe)SiO_3$ bridgmanite and (Mg,Fe)O. We found that bridgmanite has substantially higher resistance to deformation than (Mg,Fe)O.

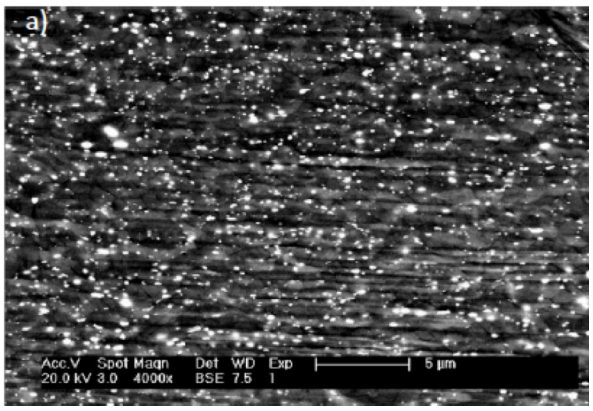

SEM micrograph of a deformed bridgmanite + (Mg,Fe)O aggregate. Dark regions are bridgmanite and light grey regions are (Mg,Fe)O. Bright spots are metallic Fe.
Conditions of deformation are P=27 GPa, T=2130 K, strain-rate ~10^{-5} s^{-1}.

Effect of Fe content on Olivine Viscosity at High P and Implication for the Martian Mantle

P. Raterron[1,2,3], C. Holyoke[4], L. Tokle[2], N. Hilairet[1], S. Merkel[1], G. Hirth[2] and D. Weidner[3]

[1]UMET, CNRS, Université de Lille, France; [2]DEEPS, Brown University, RI ; [3]Geosciences, Stony Brook University, NY; [4] Geosciences, Universty of Akron, OH

The upper parts of the mantle of rocky planetary bodies are olivine-rich, with Fe/(Mg+Fe) ratios (Fe#) lower than ~2% for Mercury, up to 25-30% for Mars, and intermediate compositions for the Earth, the Moon and Venus. Olivine represents more than 60 wt.% of the Martian upper mantle [1], where pressure (P) and temperature (T) reach 13.5 GPa and 1700 K at 1100-km depth. Results from experiments carried out at low pressure (~ 0.3 GPa) indicate that increasing Fe content dramatically decreases olivine viscosity [2]. These data suggest that the Martian upper mantle may be ~10 times less viscous than the Earth's at the same conditions. Whether such a weakening occurs at the high pressures relevant to Mars interior is unknown. We, thus, carried out deformation experiments in the D-DIA at NSLS X17B@ and APS 6-BM-B synchrotron beamlines on olivine polycrystals with various compositions along the forsterite-fayalite joint. Run P and T were within 2.5 – 8.0 GPa and 1073 – 1573 K, and strain rate was in the range 0.2 – 14 $\times 10^{-5}$ s^{-1}. Dry specimens with different iron contents, chemically separated from each other by Ni disks, were deformed two by two in order to compare their rheology. Strain rates and the applied stress were measured in situ by X-ray imaging and diffraction, as described elsewhere [3].

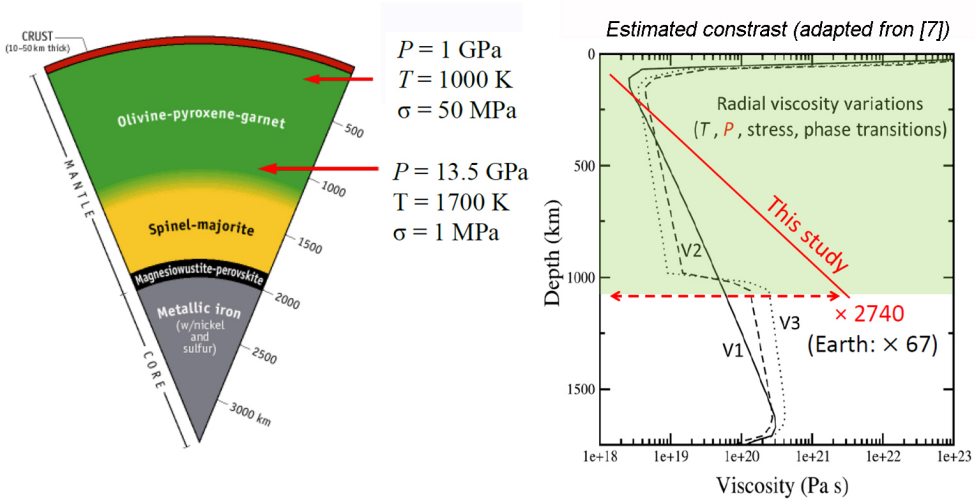

The contrast in effective viscosity between Fe-rich olivine and Fe-poor olivine is much lower at high pressure than observed at low pressure (i.e., 300 MPa, [2]). This observation is partly explained by the different strain-rate sensitivities to stress and pressure variations of olivines with different iron contents, which translate in classical power laws into different stress exponents (n) and activation volumes (V^*). By carrying out stress-step and pressure-step experiments, we observed that n and V^* increase with Fe content. A consistent increase of the n value with olivine Fe content is also observed at low P (a review in [4]). Applying these results to the interior of Mars, with an olivine Fe-content (Fe #) estimated to between 25 and 30 %, and assuming reasonable values for mantle stresses (Figure), we conclude that the viscosity increases with depth in the Martian upper mantle could be up to a factor of 40 times more than estimated in the Earth. Such a strong increase in viscosity may have critical consequences for Mars' mantle convection mode.

[1] Khan A. & Connolly J.A.D. (2008) *JGR, 113,* E07003. [2] Zhao Y.-H. et al. (2009) *EPSL*, *287,* 229-240. [3] Raterron P. & Merkel S. (2009) *J. Synchr. Rad., 16,* 748-756 ; [4] Bollinger C. et al. (2014) *PEPI*, *228,* 211-219.

This work is supported by the National Science Foundation (NSF) CSEDI grant EAR-1606793. The NSLS X17-B2 and the APS 6BM-B beamline, respectively was and is supported by the Consortium for Materials Properties Research in Earth Sciences (COMPRES) [NSF EAR 06-49658].

Ultrasonic Acoustic Velocities During Partial Melting of the Mantle Peridotite, KLB-1 (submitted to JGR, 2017)

Donald J. Weidner, Li Li, Matthew Whitaker, Richard Triplett

We have measured V_P and V_S as a function of temperature as KLB-1 begins to melt. The two sound speeds, along with the bulk sound velocity, are illustrated in Figure 1. We find that the values of $\partial \ln V_S / \partial \ln V_B$ were all significantly lower than those calculated by [*Hammond and Humphreys*, 2000] for all melt shapes that they considered implying that the change in bulk modulus was much greater than the classic mixing model would predict. Both our data and the recent data by [*Chantel et al.*, 2016] for partial melts in a system of olivine + basalt are incompatible with the mixing model in this metric, but are compatible with the dynamic melting model in which the stress of the acoustic wave drives the material back and forth between the melt and the solid following the phase equilibrium conditions as proposed by [*Anderson*, 1989; *L Li, Donald J. Weidner*, 2008; *Vaisnys*, 1968]. This model requires sufficiently fast kinetics for this to be effective.

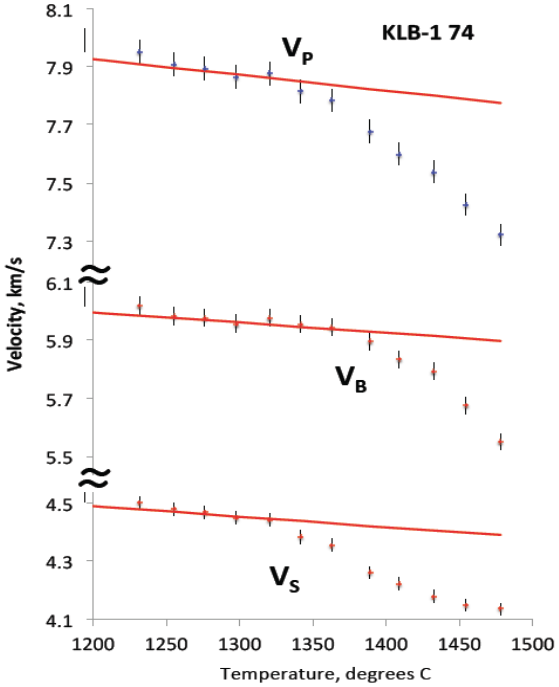

Figure 1. Measured acoustic velocities for KLB-1 as a function of temperature. The longitudinal velocity (V_P), shear velocity (V_S), and bulk sound velocity (V_B) are illustrated as a function of temperature. Error bars of 0.5% includes the estimated uncertainty of sample length. The red lines indicate estimates of the temperature dependence of velocities. The slope of these lines comes from the room-pressure temperature derivative of -0.00036 km/(sec deg) for S waves and -0.00054 km/(sec deg) for P waves for San Carlos olivine calculated from [*Anderson*, 1995]. The validity of this estimate was validated in similar runs that did not encounter partial melting.

Anderson, D. L. (1989), *Theory of the Earth*, 382 pp., Blackwell Scientific Publications.

Chantel, J., G. Manthilake, D. Andrault, D. Novella, T. Yu, and Y. B. Wang (2016), Experimental evidence supports mantle partial melting in the asthenosphere, *Science Advances*, *2*(5), doi:10.1126/sciadv.1600246.

Hammond, W. C., and E. D. Humphreys (2000), Upper mantle seismic wave velocity: Effects of realistic partial melt geometries, *Journal of Geophysical Research-Solid Earth*, *105*(B5), 10975-10986.

Li, L., Donald J. Weidner (2008), Effect of Phase Transitions on Compressional-Wave Velocites in the Earth's Mantle, *Nature 454* 984.

Vaisnys, J. R. (1968), Propagation of acoustic waves through a system undergoing phase transformations, *Journal of Geophysical Research*, *73*(24), 7675-7683.

DIASCoPE: Directly Integrated Acoustic System Combined with Pressure Experiments – A new method for fast acoustic velocity measurements at high pressure

Matthew L. Whitaker[1,*], Kenneth J. Baldwin[1], William R. Huebsch[1]
[1]Mineral Physics Institute, Stony Brook University, Stony Brook, NY 11794-2100 USA

A new experimental system to measure elastic wave velocities in samples *in situ* under extreme conditions of pressure and temperature in a multi-anvil apparatus has been installed at Beamline 6-BM-B of the Advanced Photon Source at Argonne National Laboratory. This system allows for measurement of acoustic velocities via ultrasonic interferometry, and makes use of the synchrotron beam to measure sample densities via X-ray diffraction and sample lengths using X-radiographic imaging. This system is fully integrated into the automated software controls of the beamline and is capable of collecting robust data on elastic wave travel times in less than one second, which is an improvement of more than one to two orders of magnitude over existing systems. Moreover, this fast data collection time has been shown to have no effect on the obtained travel time results. This allows for more careful study of time-dependent phenomena with tighter snapshots in time of processes that would otherwise be lost or averaged out in other acoustic measurement systems.

The figure to the right shows quite clearly that the P-wave travel times are longer in the FeS-IV phase than in the FeS-III phase. Moreover, the travel times are even longer while this phase transition is taking place than when either phase is the sole stable structure, as is shown by the shift of the light gray signal to the right of the other two. Previously existing systems for ultrasonic velocity measurement at high pressures that take on the order of ~180 seconds to collect data would have easily been able to collect data on the FeS-III (dark gray) and FeS-IV (black) phases. However, their prohibitively long collection times means that the increase in travel time that is observed while the phase transition is actively occurring would be lost and averaged into the longer-term stable signal of the single phase end products.

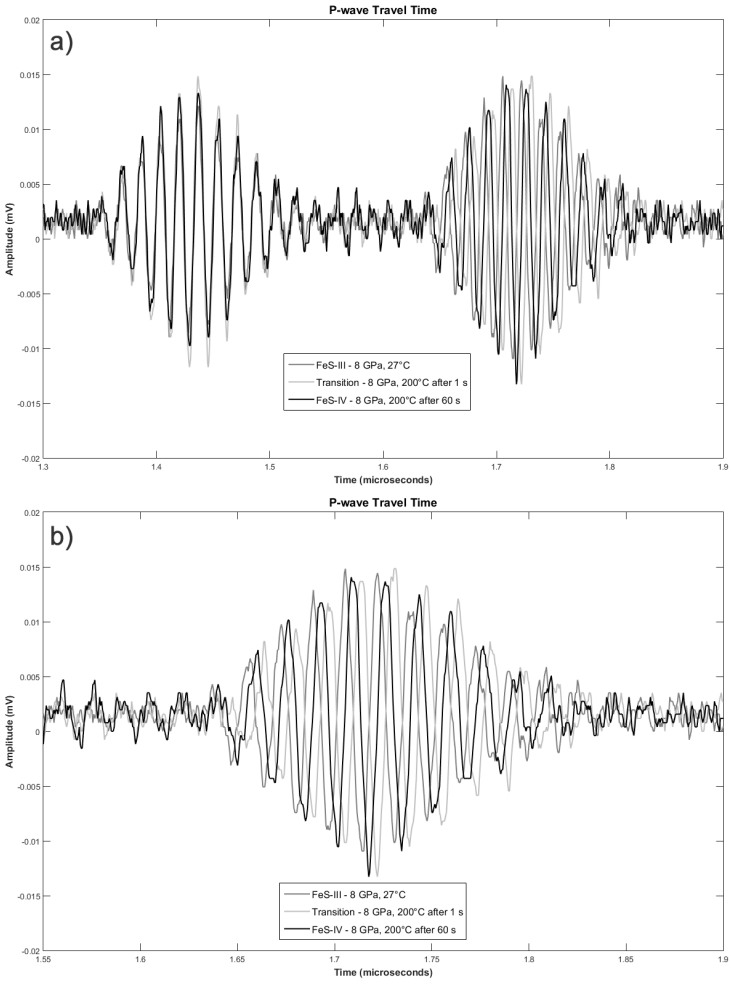

Whitaker, M.L., Baldwin, K.J., and Huebsch, W.R. (2017) DIASCoPE: Directly Integrated Acoustic System Combined with Pressure Experiments – A new method for fast acoustic velocity measurements at high pressure. Review of Scientific Instruments, 88, 034901. DOI 10.1063/1.4977596

Appendix II Publications (NSLS X17B2 & APS 6BM-B)

2012

1. Akdogan, E., I Savkhyildiz, B Berke, Z Zhong, L Wang, D Weidner, M Croft, T Tsakalakos (2012), Pressure Effects on Phase Equilibria and Solid Solubility in MgO-Y2O3 Nanocomposites, *J. Appl. Phys.*, *111 (5), Article Number 053506*
2. Bollinger, C., S. Merkel, and P. Raterron (2012), In situ quantitative analysis of stress and texture development in forsterite aggregates deformed at 6 GPa and 1373 K, *Journal of Applied Crystallography*, *45*, 263-271.
3. Botez C, R Tackett, J Hermosillo, J Zhang, Y Zhao, L Wang (2012), High Pressure Synchrotron X-ray Diffraction Studies of Superprotonic Transitions in Phosphate Solid Acids, *Solid State Ionics*, *213* (58-62).
4. Dobson, D. P., Richard McCormack, Simon A. Hunt, Michael W. Ammann, Donald Weidner, Li Li, and L. Wang (2012), The relative strength of perovskite and post-perovskite in the system NaCoF3, *Mineralogical Magazine*, *76* 925-932
5. Girard, J., J. H. Chen, and P. Raterron (2012), Deformation of periclase single crystals at high pressure and temperature: Quantification of the effect of pressure on slip-system activities, *Journal of Applied Physics*, *11, 112607*.
6. Hunt, S. A., D. R. Davies, A. M. Walker, R. J. McCormack, A. S. Wills, D. P. Dobson, and L. Li (2012), On the increase in thermal diffusivity caused by the perovskite to post-perovskite phase transition and its implications for mantle dynamics, *Earth and Planetary Science Letters*, *319 - 320*, 96-103.
7. Jing Z, Karato S, et al (2012), Effects of H2O on the density of silicate melts at high pressures: Static experiments and the application of a hard-sphere model of equation of state, *Geochim. Cosmochim. Acta.*, *85: 357-372.*
8. Karato, S. (2012), On the origin of the asthenosphere *Earth, Planet. Sci. Lett.*, *321/322: 95-103*.
9. Li, L., and D. J. Weidner (2012), Anelasticity and Transient Creep in NaMgF3 Perovskite at High Pressure, *Physics of the Earth and Planetary Interior*, *194-195*, 98-106.
10. Otsuka, K. and Karato., S.-I. (2012), Deep penetration of molten iron into the mantle caused by the morphological instability, *Nature*, *492: 243-247*.
11. Raterron, P., J. Girard, and J. H. Chen (2012), Activities of olivine slip systems in the upper mantle, *Physics of the Earth and Planetary Interiors*, *200*, 105-112.
12. Wang, D., Karato, S., and Li, Z-Y (2012), Influence of hydrogen on the electronic state of olivine: Implications for electrical conductivity *Geophys. Res. Lett.*, *39*. *Article Number L06306, doi: 10.1029/2012GL051046*
13. Wang, D., Guo, Y., Yu, Y. and Karato, S. (2012), Electrical conductivity of amphibole-bearing rocks: Influence of dehydration., *Contrib. Mineral. Petrol.*, *164: 17-25*.
14. Wang, S., X Yu, J Zhang, M Chen, J Zhu, L Wang, D He, Z Lin, R Zhang, et. al. (2012), Experimental invalidation of phase-transition-induced elastic softening in CrN, *Phys. Rev. B: Condens. Matter*, *86, 064111*
15. XH Yu, JZ Zhang, YY Zhang, LP Wang, and YS Zhao (2012), Comparative Studies of Yield Strength and Elastic Compressibility Between Nanocrystalline and Bulk Cobalt, *J. Appl. Phys.*, *111, 113506*.
16. Yu, X., Raterron, P., Zhang, J., Lin, Z., Wang, L., Zhao, Y. (2012), Constitutive Law and Flow Mechanism in Diamond Deformation, *Scientific Reports*, *2, 876*.

2013

1. Akdogan, E., I Savkliyildiz, H Bicer, W Paxton, F Toksoy, Z Zhong, T Tsakalakos (2013), Anomalous Lattice Expansion in Yttria Stabilized Zirconia Under Simultaneous Applied Electric and Thermal Fields: A Time-Resolved In Situ Energy Dispersive X-ray Diffractometry Study With an Ultrahigh Energy Synchrotron Probe, *J. Appl. Phys.*, *113(23), 233503*
2. Chen, H., Tian Yu, Peng Gao, Jianming Bai, Jing Tao, Trevor A. Tyson, Liping Wang, and Roger Lalancette (2013), Synthesis and structure of perovskite ScMnO3, *Inorg. Chem.*, *52, 9692-9697*
3. Deyhim, A., E Every (2013), Development of a Custom High Precision Motion System to Manipulate a 7 Ton Press., *J Phys.: Conf. Ser.*, *425, 132014*
4. Farla, R., Karato, S., and Cai, Z. (2013), Role of orthopyroxene in rheological weakening of the lithosphere via dynamic recrystallization, *Proc. Nat. Acad. Sci.*, *10: 16355-16360*
5. Girard, J., J Chen, P Raterron, C Holyoke (2013), Hydrolytic weakening of olivine at mantle pressure: Evidence of [100] (010) slip system softening from single-crystal deformation experiments, *Physics of Earth and Planetary Interiors*, *216*, 12-20.
6. Grott, M., Baratoux, D., Hauber, E., Sautter, V., Mustard, J., Gasnault, O., Ruff, S., Karato, S., Debaile, V., Knapmeyer, M., Sohl, F., Van Hoolst, T., Breuer, D., Morschhauer, A. and Toplis, M.J. (2013), Long-term evolution of eth Martian crust-mantle system, *Space Science Review*, *174: 49-111*.
7. Gwanmesia, G. D., Liping Wang, Adaire Heady, and Robert C. Liebermann (2013), Elasticity and sound velocities of polycrystalline grossular (Ca3Al2Si3O12) at simultaneous high pressures and high temperatures, *Physics of the Earth and Planetary Interiors*, *228, 80-87*
8. Hunt, S. A., Lindsay-Scott, A., Wood, I. G., Ammann, M. W. and Taniguchi, T (2013), The P-V-T equation of state of CaPtO3 post-perovskite, *Physics and Chemistry of Minerals*, *40, 73 – 80*.
9. Hustoft, J., G. Amulele, J. Ando, K. Otsuka, Z. Du, Z. Jing, and S. Karato (2013), Plastic deformation experiments to high strain on mantle transition zone minerals wadsleyite and ringwoodite in the rotational Drickamer apparatus, *Earth and Planetary Science Letters*, *361*, 7-15.
10. Karato, S., Wang, D. (2013), Electrical conductivity of minerals and rocks in *Physics and Chemistry of the Deep Earth*, edited by S. Karato, pp. 145-182, Wiley-Blackwell.
11. Karato, S. (2013), Geophysical constraints on the water content in the lunar mantle and its implication for the origin of the Moon, *Earth Planet Sci. Lett.*, *384: 144-153*.
12. Karato, S. (2013), Theory of isotope diffusion in materials with multiple species and its implications for hydrogen-enhanced electrical conductivity in olivine *Phys. Earth Planet. Inter.*, *219: 49-55.*
13. Karato, S. (2013), Rheological properties of minerals and rocks, in *Physics and Chemistry of the Deep Earth*, edited by S. Karato, pp. 94-144, Wiley-Blackwell, New York.
14. Li, L., and D. J. Weidner (2013), Effect of Dynamic Melting on Acoustic Velocities in a Partially Molten Peridotite, *Physics of the Earth and Planetary Interior*, *222*, *1-7*.
15. Olugboji, T. M., Karato, S., and Park, J. (2013), Structures of the oceanic lithosphere-asthenosphere boundary: Mineral physics modeling and seismological signatures, *Geochem., Geophys., Geosyst. 14 (4), 880-901, doi: 10.1002/ggge.20086*
16. Otsuka, K., Longo, M., McCammon, C. and Karato, S. (2013), Ferric iron content of ferropericlase as a function of composition, oxygen fugacity, temperature and pressure: Implications for the redox conditions during diamond formation in the lower mantle, *Earth Planet. Sci. Lett.*, *365: 7-16*.

17. Raterron, P., S Merkel, C Holyoke (2013), Axial temperature gradient and stress measurements in the deformation-DIA cell using alumina pistons, *Review of Scientific Instruments*, *84*(043906).
18. Savklıyıldız, I., E.K. Akdogan, Z. Zhong, L. Wang, D. Weidner, M. Vaughan, M.C. Croft, and T. Tsakalakos (2013), Phase transformations in hypereutectic MgO-Y2O3 nanocomposites at 5.5GPa, *Journal of Applied Physics*, *113, 203520*
19. Wang, D., Karato, S., and Jiang, Z. (2013), An experimental study on the influence of graphite on the electrical conductivity of olivine aggregates, *Geophys. Res. Lett.40 (10) 2028-2032, doi:10.1002/grl.50471*
20. Weidner, D. J., and L. Li (2013), Theory & Practice - Methods for the Study of High P/T Deformation & Rheology, in *Treatise on Geophysics, 2nd Edition*, edited by L. Stixrude and D. P. Geoffrey, Elseviere.
21. Xu, L., S Mei, NA Dixon, Z Jin, A Suzuki, D.L. Kohlstedt (2013), Effect of water on rheological properties of garnet at high temperatures and pressures, *Earth Planet. Sci. Lett.*, *379, 158-165*
22. Zhang, J. Z., JL; Velisavljevic, N; Wang, LP; Zhao, YS (2013), Thermal equation of state and thermodynamic Gruneisen parameter of beryllium metal, *Journal of Applied Physics*, *114, 173509*
23. Zhu, J., Zhao, YS, et al (2013), Temperature and pressure effects of multiferroic Bi2NiTiO6 compound, *J. Appl. Phys.*, *113 (14), 143514*.

2014

1. Bollinger, C., Raterron, P., Cordier, P., Merkel, S. (2014), Polycrystalline olivine rheology in dislocation creep: revisiting experimental data to 8.1 GPa, *Phys. Earth Planet. Int.*, *228, 211-219.*
2. Chen, J. C., T Yu, S Huang, J Girard, X Liu (2014), Compressibility of Liquid FeS Measured Using X-ray Radiograph Imaging, *Phys. Earth Planet. Interiors*, *228, 294-299*
3. Dai, L., Karato, S. (2014), The effect of pressure on hydrogen-assisted electrical conductivity of olivine: implications for the conductivity jump at 410-km, *Phys. Earth Planet. Inter.*, *232: 51-56.*
4. Dai, L., Karato, S. (2014), Influence of FeO and H on the electrical conductivity of olivine, *Phys. Earth Planet. Inter., 237, 73-79*
5. Dai, L., Karato, S. (2014), The effect of oxygen fugacity on hydrogen-assisted electrical conductivity of olivine: implications for the mechanism of conduction, *Phys. Earth Planet. Inter.*, *232: 57-60.*
6. Dai, L., Karato, S. (2014), High and highly anisotropic electrical conductivity of the asthenosphere caused by hydrogen diffusion in olivine *Earth and Planetary Science Letters, 408, 79-86*
7. Du, W., L. Li, and D. J. Weidner (2014), Experimental observation on grain boundaries affected by partial melting and garnet forming phase transition in KLB1 peridotite, *Physics of the Earth and Planetary Interior (228), 287-293*.
8. Hunt, S. A., Weidner, D. J., McCormack, R. J., Whitaker, M. L., Bailey, E., Li, L., Vaughan, M. T., Dobson, D. P. (2014), Deformation T-Cup: A new multi-anvil apparatus for controlled strain-rate deformation experiments at pressures above 18 GPa. , *Rev. Sci. Instrum.*, *85, 085103*.
9. Karato, S. (2014), Asymmetric shock heating and the terrestrial magma ocean origin of the Moon, *Proceedings of the Japan Academy*, *B90: 97-103.*
10. Karato, S. (2014), Does partial melting explain geophysical anomalies? *Physics of the Earth and Planetary Interiors*, *228*, 300-306.
11. Karato, S. (2014), Some remarks on the models of plate tectonics on terrestrial planets: From the view-point of mineral physics, *Tectonophysics*, *631*, 4-13.
12. Kung, J., B Li. (2014), Lattice Dynamic Behavior of Orthoferrosilite (FeSiO3) toward Phase

Transition under Compression, *J. Phys. Chem. C 118(23),* , 12410-12419
13. Li, B., R Liebermann (2014), Study of the Earth's Interior Using Measurements of Sound Velocities in Minerals by Ultrasonic Interferometry, *Phys. Earth Planet. Interiors*, *233, 135-153*
14. Li, L., and D. Weidner (2014), Detection of melting by X-ray imaging at high pressure, *Review of Scientific Instruments, 85 (6) Article Number: 065104 doi:10.1063/1.4880730*
15. Lord, O. T., E. Wan, S. A. Hunt, A. M. Walker, J. Santangeli, M. J. Walter, D. P. Dobson, I. G. Wood, L. Vočadlo, G. Morard and M. Mezouar (2014), The NiSi melting curve to 70 GPa, *Physics of the Earth and Planetary Interiors*, *233, 13-23*.
16. Miyagi, L., G. Amulele, K. Otsuka, Z. Du, R. Farla, and S. Karato (2014), Plastic anisotropy and slip systems in ringwoodite deformed to high strain in the rotational Drickamer apparatus, *Physics of the Earth and Planetary Interiors*, *228*, *245-253*.
17. Raterron, P., Detrez, F., Castelnau, O., Bollinger C., Merkel, S., Cordier, P. (2014), Multiscale Modeling of Upper Mantle Plasticity: from Single-Crystal Rheology to Multiphase Aggregate Deformation, *Phys. Earth Planet. Int.*, *228, 232-243.*
18. Selway, K. M., Yi, J. and Karato, S. (2014), Water content of the Tanzanian lithosphere: Implications for cratonic growth and stability, *Earth Planet. Sci. Lett.*, *388: 175-186*.
19. Simon A. Hunt, Donald J. Weidner, Richard J. McCormack, Matthew Whitaker, Edward Bailey, Li Li, Michael T. Vaughan, and D. P. Dobson (2014), Deformation T-Cup: A new apparatus for high temperature controlled strain-rate deformation experiments tested to 18GPa. *Review of Scientific Instruments*, *85(8), 8.*
20. Wang, S. Y., XH; Zhang, JZ; Zhang, Y; Wang, LP; Leinenweber, K; Xu, HW; Popov, D; Park, C; Yang, WG; He, DW; Zhao, YS (2014), Crystal structures, elastic properties, and hardness of high-pressure synthesized CrB2 and CrB4., *JOURNAL OF SUPERHARD MATERIALS 36, 279-287*
21. Zhang, J., J Han, J Zhu, Z Lin, M Braga, L Daemen, L Wang, Y Zhao (2014), High Pressure-High Temperature Synthesis of Lithium-rich Li3O(Cl, Br) and Li3 − xCax/2OCl Anti-Perovskite Halides, *Inorg. Chem. Comm.*, *48, 140-143*
22. Zou, Y., X Qi, X Wang, T Chen, X Li, D Welch, B Li (2014), High-pressure Behavior and Thermoelastic Properties of Niobium Studied by in situ X-ray Diffraction, *J. Appl. Phys.*, *116, 013516*.

2015

1. Bollinger, C., Merkel, S, Cordier, P., Raterron, P. (2015) Deformation of forsterite polycrystals at mantle pressure: Comparison with Fe-bearing olivine and the effect of iron on its plasticity, *Phys. Earth Planet. Int., 240, 95-104.*
2. Karato, S., 2015. Water in the evolution of Earth and other terrestrial planets, *Treatise on Geophysics,* v. 9, "*Evolution of the Earth*" (edited by D.J. Stevenson), Elsevier, 105-144.
3. Otsuka, K., and Karato, S., 2015. The influence of ferric iron and hydrogen on the Fe-Mg inter-diffusion in (Mg,Fe)O ferropericlase in the lower mantle, *Physics and Chemistry of Minerals, 42: 261-273.*
4. Farla, R., Amulele, G., Girard, J., Miyajima, N. and Karato, S., (2015). High pressure and temperature deformation experiments on polycrystalline wadsleyite using the rotational Drickamer apparatus, *Physics and Chemistry of Minerals, 42: 541-558.*
5. Li, L. and D.J. Weidner, In situ analysis of texture development from sinusoidal stress at high pressure and temperature. *Review of Scientific Instruments, 2015. 86(12) 125106.*

6. Burnley, P. C., 2015, Elastic Plastic Self Consistent (EPSC) Modeling of Plastic Deformation in Fayalite Olivine. *American Mineralogist. V. 100, p.1424 – 1433, OSTI ID 1332345, doi: 10.2138/am-2015-5234CCBYNCND*
7. Karato, S., 2015. Some notes on hydrogen-related point defects and their role in the isotope exchange and electrical conductivity in olivine, *Physics of the Earth's Interior, 238: 94-98.*
8. Karato, S., Olugboji, T., and Park, J. (2015), Mechanisms and geological significance of the mid-lithosphere discontinuity in the continents, *Nature Geoscience*. *8, 509-514*
9. Otsuka, K., and Karato, S. (2015), The influence of ferric iron and hydrogen on the Fe-Mg inter-diffusion in (Mg,Fe)O ferropericlase in the lower mantle, *Physics and Chemistry of Minerals, 42 (4) 261-273*
10. Karato, S. (2014), Water in the evolution of Earth and other terrestrial planets, Treatise on Geophysics, in *Evolution of the Earth*, edited by e. b. D. J. Stevenson, Elsevier, P105-144
11. Wang, SM; Zang, CP; Wang,YK; Wang, LP; Zhang, JZ; Childs, C; Ge, H; Xu, HW; Chen, HY; He, DW; Zhao, YS (2015) Revisit of pressure-induced phase transition in PbSe: crystal Structure, and thermoelastic and electrical properties. *Inorganic Chemistry, 54, 4981-4989; DOI: 10.1021/acs.inorgchem.5b00591.*
12. Weidner, D.J. and L. Li, Kinetics of melting in peridotite from volume strain measurements. *Physics of the Earth and Planetary Interiors, 2015.* ***246****: p. 25-30.*
13. Zhang, JZ; Zhu, JL; Wang, LP; Zhao, YS (2015) A new lithium-rich anti-spinel in Li–O–Br system. *Chemical Communications, 51, 9666-9669; doi: 10.1039/c5cc01109d.*
14. Wang, SM, Ge, H; Sun, SL; Zhang, JZ; Liu, FM; Wen, XD; Yu, XH; Wang, LP; Zhang, Y; Xu, HW; Neuefeind, JC; Qin, ZF; Chen, CF; Jin, CQ; Li, YW; He, DW; Zhao, YS (2015) A new molybdenum nitride catalyst with rhombohedral MoS2 structure for hydrogenation applications. *JOURNAL OF THE AMERICAN CHEMICAL SOCIETY, 137, 4815-4822; DOI: 10.1021/jacs.5b01446*
15. JM. Bai, J. Hong, H. Chen, J. Graetz, F. Wang, "Solvothermal Synthesis of LiMn1-xFexPO_4 Cathode Materials: A Study of Reaction Mechanisms by Time-Resolved in Situ Synchrotron X-ray Diffraction", *Journal of Physical Chemistry C, 119 (2015) 2266*
16. Y. Li, YT. Zou, T. Chen, XB. Wang, XT. Qi, H. Chen, JG. Du, BS. Li, "P-V-T equation of state and high-pressure behavior of $CaCO_3$ aragonite", *American Mineralogists*, *100 (2015) 2323*

2016

1. Bollinger, C., P., Raterron, P. Castelnau, O., Detrez, F., Merkel, S. (2016) Textures in Deforming Forsterite Aggregates up to 8 GPa and 1673 K, *Phys. Chem. Miner., 43, 409-417*
2. Raterron, P., Fraysse, G., Girard, J., Holyoke, C.W. III (2016) Strength of orthoenstatite single crystals at mantle pressure and temperature and comparison with olivine, *Earth and Planetary Science Letters, 450, 326-336.*
3. Liu, Z., Park, J. and Karato, S., (2016). Seismological detection of low velocity anomalies surrounding the mantle transition zone in Japan subduction zone, *Geophysical Research Letters*, *43: 2480-2487.*
4. Karato, S., 2016. Physical basis of element partitioning: A review, *American Mineralogist, 101 (12) 2577-2593*

5. Masuti, S., Barbot, S.D., Karato, S., Feng, L. and Banerjee, P., (2016). Upper mantle water stratification inferred from observations of the 2012 Indian Ocean earthquake, *Nature,* 538: 373-377.
6. Girard, J., Amulele, G., Farla, R. and Karato, S., 2016. Shear deformation of bridgmanite and ferropericlase aggregates at lower mantle conditions, *Science, 351: 144-147.*
7. Olugboji, T., Park, J., Karato, S., Kawakatsu, H. and Shinohara, M. (2016), The nature of the lithosphere-asthenosphere boundary in the normal oceanic upper mantle, *Geochemistry, Geophysics and Geosystems, 17 (4) 1265-1282*
8. Qiang He, Xi Liu, Baosheng Li, Liwei Deng, Wei Liu, Liping Wang (2016) Thermal equation of state of a natural kyanite up to 8.55 GPa and 1273 K. *Matter and Radiation at Extremes; 1 (5) 269-296*
9. Jianzhong Zhang, Nenad Velisavljevic, Jinlong Zhu and Liping Wang (2016) Equation of state and thermodynamic Grüneisen parameter of monoclinic 1,1-diamino-2,2-dinitroethylene. *J. Phys.: Condens. Matter 28 395402; doi:10.1088/0953-8984/28/39/395402*
10. Pei Wang, Yonggang Wang, Liping Wang, Xinyu Zhang, Xiaohui Yu, Jinlong Zhu, Shanmin Wang, Jiaqian Qin, Kurt Leinenweber, Haihua Chen, Duanwei He & Yusheng Zhao (2016) Elastic, magnetic and electronic properties of iridium phosphide Ir2P. *Scientific Reports, 6, Article number: 21787; doi:10.1038/srep21787*
11. Shanmin Wang, Xiaohui Yu, Jianzhong Zhang, Liping Wang, Kurt Leinenweber, Duanwei He, and Yusheng Zhao (2016) Synthesis, hardness, and electronic properties of stoichiometric VN and CrN. *Crystal Growth & Design, 16 (1), 351–358; doi: 10.1021/acs.cgd.5b01312*
12. Wang, YJ; Liu, ZTY; Khare, SV; Collins, SA; Zhang, JZ; Wang, LP; Zhao, YS (2016) Thermal equation of state of silicon carbide. *Applied Physics Letters, 108, 061906; doi: 10.1063/1.4941797*
13. Dobson, D.P., Hunt, S.A., Ahmed, J., Lord, O.T., Wann, E., Santangeli, J., Wood, I.G., Vocadlo, L., Walker, A., Mueller, H.J., Lathe, C., Whitaker, M.L., Morard, G., and Mezouar, M. (2016) The Phase Diagram of NiSi Under the Conditions of Small Planetary Interiors. Physics of the Earth and Planetary Interiors, 261, 196-206. DOI 10.1016/j.pepi.2016.10.005
14. Hunt, S. A., Walker, A.M. and Mariani, E. (2016) In-situ measurement of fabric development rate in CaIrO3. *Physics of the Earth and Planetary Interiors, 259, 91-104 doi: 10.1016/j.pepi.2016.05.007*
15. Woerner, WR; Qian, GR; Oganov, AR ; Stephens, PW; Dharmagunawardhane, HAN; Sinclair, A; Parise, JB , 'Combined Theoretical and in Situ Scattering Strategies for Optimized Discovery and Recovery of High-Pressure Phases: A Case Study of the GaN-Nb2O5 System', *Inorganic Chemistry, 55 (2016) 3384*
16. T. Wu, T. A. Tyson, H. Chen, P. Gao, T. Yu, Z. Chen, Z. Liu, K. H. Ahn, X. Wang and S.-W. Cheong, "Pressure Dependent Structural Changes and Predicted Electrical Polarization in Perovskite $RMnO_3$", *Journal of Physics Condensed Matter*, *28 (2016) 056005*

2017

1. Cheung, S. N. C.; Weidner, D. J.; Li, L.; Meredith, P. G.; Chen, H.; Whitaker, M. L.; Chen, X. (2017) Stress distribution during cold compression of a quartz aggregate using

synchrotron X-ray diffraction: observed yielding, damage and grain crushing. *Journal of Geophysical Research (Solid Earth), 122 (4) 2724-2735*

2. Whitaker, M.L., Baldwin, K.J., and Huebsch, W.R. (2017) DIASCoPE: Directly Integrated Acoustic System Combined with Pressure Experiments – A new method for fast acoustic velocity measurements at high pressure. *Reviews of Scientific Instruments. 88 (3) 034901* DOI 10.1063/1.4977596
3. Farla R., Amulele G., Girard J., Miyajima N., Karato SI., (2017) High-pressure and high-temperature deformation experiments on polycrystalline wadsleyite using the rotational Drickamer apparatus (vol 42, pg 541, 2015), *Physics and Chemistry of Minerals* 44 (3) 235

Abstracts (there are many more that this)

1. Rucks, M.J., Glotch, T.D., Whitaker, M.L., and Parise, J.B. (2017) Preliminary Investigation of Tissintite Formation Using in situ Synchrotron X-Ray Diffraction and Multi-Anvil Techniques. Lunar and Planetary Science Conference, XLVIII, Abstract #2427
2. L. Tokle, G. Hirth, P. Raterron, N. Dygert, Y. Liang, C. W. Holyoke , "The Pressure and Mg Dependence of Ilmenite and Ilmenite-olivine Aggregates Rheology: Implications for Lunar Cumulate Mantle Overturn*", Lunar Planetary Science Conference Abstracts, April, 2017*
3. P. Raterron, L. Tokle, N. Hilairet, S. Merkel, G. Hirth, D. Weidner , "Effect of Fe Content on Olive Viscosity and Implications for the Martian Mantle", *Lunar Planetary Science Conference Abstracts, April, 2017*
4. Rucks, M.J., Glotch, T.D., Whitaker, M.L., and Parise, J.B. (2017) Investigation of Tissintite Formation Using in situ Synchrotron X-Ray Diffraction and Multi-Anvil Techniques. 80th Annual Meeting of the Meteoritical Society, LPI Contrib. No. 1987, Abstract #6325.

Submitted to Refereed Journals

1. S. Kaboli, P. C. Burnley, G. Xia and H. W. Green II "Pressure dependence of creep in forsterite olivine: comparison of measurements from the D-DIA and Griggs apparatus", *submitted to GRL*
2. S. Kaboli and P. Burnley, "ECCI, EBSD and EPSC Characterization of Rhombohedral Twinning in Polycrystalline α-Alumina Deformed in the D-DIA Apparatus", *Submitted to Journal of Applied Crystallography*
3. Weidner, D., L. Li, M. Whitaker, R. Triplett, "Ultrasonic Acoustic Velocities During Partial Melting of a Mantle Peridotite KLB-1", *submitted to J. Geophys, Res.*

Papers in Preparation

1. LP Wang, JZ Zhang, P Wang, SM Wang, YS Zhao, HY Chen, "Effect of Electronic Disordering on the Thermal Equation State of Magnetite", *to be submitted*
2. P Wang, K Kisslinger, HY Chen, LP Wang, "Flow mechanism and Constitutive Law of Superhard Nanocrystalline and Microstalline cBN: In-Situ Deformation Study at Simultaneous High-Pressure and Temperature", *to be submitted to Physical Review Letters*
3. Dobson DP, Hunt SA, Schardong L, Thomson AR, Ezad IS, Bailey, E, Walker AM, Lord, OT, Marquardt, K, Melai, C, Whitaker, ML and Weidner, DJ, "Pressure-induced grain-

boundary stiffening and suppression of anelasticity in silicate minerals", *to be submitted to PNAS*

4. Cecilia S N Cheung, Donald J Weidner, Li Li, Philip Meredith, Haiyan Chen, Matthew L Whitaker, Xianyin Chen, Stress distribution during cold compression of rocks and mineral aggregates using X-ray diffraction at 6BM, *to be submitted to JoVE*
5. Simon A. Hunt, Matthew L. Whitaker, Edward Bailey, Elisabetta Mariani, Camelia Stan, David P. Dobson, The effect of Si-coordination on the rheology of SiO_2 polymorphs, *in preparation for GRL*
6. Rucks, M.J., Whitaker, M.L., Glotch, T.D., and Parise, J.B. (in prep) Tissintite Formation and its Implications for Impact Events. *To be submitted to Nature*
7. Whitaker, M.L. (in prep) Observation of elastic modulus softening during phase transition. *To be submitted to Science Advances*

PhD Dissertations

1. McCormack, R. (2012), The Rheological and Transport Properties of Deep Mantle Materials, Ph.D Thesis. University College London, London
2. Girard, J (2012) Effect of water on olivine single crystl plasticity: Deformation at high pressure and temperature, PhD Thesis, Florida International University
3. Bolliger, C (2013), Rhéologie de l'olivine polycristalline aux conditions du manteau supérieur : étude en D-DIA, Université de Lille (Feb 7th)
4. Dixon, N. A. (2014), Experimental Constraints on the Rheological Behavior of Olivine at Upper Mantle Conditions, Ph. D. thesis, 125 pp, Massachusetts Institute of Technology.
5. Woerner, W. R. (2015) In Situ Scattering and Modeling Approaches for the Discovery and Optimization of Novel Mineral-Inspired Materials, Stony Brook University, August
6. Wann ETH (2015) The Core Composition of Terrestrial Planets: A Study of the Ternary Fe-Ni-Si System, PhD Thesis, University College of London, London
7. Cheung, S. N. C., (2015): "Experimental deformation in sandstone, carbonates and quartz aggregate" Stony Brook University
8. Proietti, A. (2016), Rhéologie d'agrégats olivine-orthopyroxène sous haute pression, Universite Toulouse III Paul Sabatier, Toulouse, January.
9. Tercé, N. (2016), Propriétés élastiques des olivines riches en fer, Université Toulouse III Paul Sabatier, Toulouse, 10 November.
10. Zhang, G. (2016), Diffusion Creep of Enstatite at High Pressure under Hydrous Condition, State Key Laboratory of Isotope Geochemistry, Guangzhou Institute of Geochemistry, Guangzhou, China
11. Wang, X. (2016) Mantle composition and temperature of western North America revealed from in-situ velocity measurements of KLB-1 peridotite, Ph. D. Thesis, Stony Brook University
12. Dharmagunawardhane, HAN (2017) Synthesis of oxynitride materials for solar water splitting: investigations with ambient pressure and high pressure synthesis techniques, Ph. D. Thesis, Stony Brook University

MS Theses

1. Suer, T.-A. (2013), Olivine viscoelasticity in sinusoidal stress fields at mantle conditions, Stony Brook University.
2. Cline, CJ (2014), "The Effect of Single Crystal Elastic and Plastic Anisotropy on Stress and Strain Heterogeneity: Comparison of Olivine to Other Common Minerals", University of Nevada at Las Vegas

Appendix III User Statistics

Facility	X17B2		Move	6-BM-B	
Year	9/12-8/13	9/13-8/14	9/14-8/15	9/15-8/16	9/16-8/17
Beamtime proposals received	78	66	13	42	40
Proposals awarded beamtime	50	47	5	31	36
Beamtime shifts requested	936	900	153	442	366
Beamtime shifts granted	303	456	60	280	297
Oversubscription rate	309%	197%	255%	158%	123%
Distinct research group visits	72	53	6	43	57
Total number of person-visits	103	130	18	88	97
Undergraduate users	2	1	2	2	2
Graduate student users	16	25	2	10	11
Number of unique users	58	65	15	33	36

Appendix IV. Other Beamlines with Similar Agenda

The following table aggregates data on multi-anvil synchrotron facilities around the world. For the purpose of putting together this table, we included only facilities that presently have commissioned equipment that allows for deformation studies, most notably the DDIA. We have listed here technical specs and operational details for the multi-anvil programs at GSECARS at APS, Beamline ID06 at ESRF, BL04B1 at SPring-8, and the Stony Brook Multi-Anvil X-ray program at both 6-BM-B of APS and XPD-D of NSLS-II. When discussing the imaging systems, stitching refers to the process of combing multiple images in order to fully view the sample and strain markers because they do not fit in a single image, which introduces uncertainties in measurements. The final row lists unique or novel experimental techniques at each facility.

User Facility	APS	ESRF	SPring-8	SBMAX - APS & NSLS-II
Beamline	GSECARS	ID06	BL04B1	6-BM-B & XPD-D
Multi-Anvil Beamtime %	~50%	<50%	100%	~66-75%
Dedicated MAP Personnel	2 Beamline Scientists 1+ Post-Doctoral Ass.	1 Beamline Scientist 1 Post-Doctoral Ass.	2 Beamline Scientists 1+ Post-doctoral Ass.	2 Beamline Scientists
Multi-Anvil Toolings	DIA, DDIA, DDIA-30, T25, T10, P-E Cell, HP Tomo	DDIA, DIA, Kawai 100	DDIA, DIA, Kawai 100	DIA, DDIA, T25, DT25, T10, RDA, (DT10)
Beam Type	White / Mono	Mono	White / Mono	White / Mono
Image Stiching Required?	Some	Yes	No	No
Deformation Enabled?	Mono Beam Only	Mono Beam Only	Mono Beam Only	Both White and Mono
Stress Resolution	± 20-100 MPa	± 20 MPa	± 200 MPa	± 10 MPa
Conical slit	no	no	no	Yes (at APS)
Ultrasonic Collection Time	~45-180 sec	~30-180 sec	~30 sec	~1 sec
Novel or Unique Experiment Capabilities	HP Tomography, Acoustic Emission		Ultrahigh Pressure Studies (SD Anvils)	White Beam Stress/Strain, Lo frequency Q and elastic, Thermal Diffusivity, Fast Acoustic Velocities, Deformation & Rheological Properties into Lower Mantle

Appendix V. Proposed Budget and Justification

Budget June 1, 2018 - May 31, 2019 — 6BMB at APS

Item	Amount
BL scientist, Haiyan Chen	$93,000
Fringe Benefits (.41)	$38,130
Equipment	$0
Travel	$12,800
Supplies	$21,167
Shop support	$4,082
IDC (.26) - not equipment	$43,987
Total	$213,166

Budget Justification

The salary is for Haiyan Chen, the beamline scientist. We were told by Dr. Denny Mills, Associate Director of APS, that 2 beamline personnel were necessary for one full time operating end station. Thus, 1 beamline scientist is the minimum personnel for operating 50% of the beamtime (we actually get about 55%).

The travel budget for this year includes funds for the beamline scientist, to attend the COMPRES meeting ($800), costs for attending one scientific conference the beamline scientist ($2000), and support for 10 trips from New York to Chicago for PI and other staff to support the APS operation ($1000 per trip).

Materials and supplies are mainly used for sintered diamond anvils, tungsten carbide anvils, high pressure cell assemblies, and maintenance. Over the past two years, we have found the need to replace modules that convert the signal to diffraction spectra, we have needed repairs of our slits (motors and power supplies have burned out due to radiation damage), and preamps on the detector.

In the other category, we include technical support as provided by the synchrotron facility. This support is required for moving heavy objects such as the press and the RDA when Karato comes, machining, or other operation done to the installation. We included about 20 hours as an estimate at an estimated cost of $180.00/hour. We anticipate that our staff can carry out support for our high pressure equipment, but facility support is essential for hutch related operations and for safety control.